Journal Pre-proof

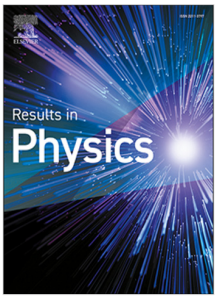

Computational investigation of an unsteady non-Newtonian and non-isothermal fluid between coaxial contracting channels: A PCM approach

Aamir Khan, Rehan A. Shah, M. Kamran Alam, Hijaz Ahmed, M. Shahzad, Sajid Rehman, Sohail Ahmed, M. Sohail Khan, Abdel-Haleem Abdel-Aty, Mohammed Zakarya

PII: S2211-3797(21)00670-7
DOI: https://doi.org/10.1016/j.rinp.2021.104570
Reference: RINP 104570

To appear in: *Results in Physics*

Received date : 1 May 2021
Revised date : 13 July 2021
Accepted date : 14 July 2021

Please cite this article as: A. Khan, R.A. Shah, M.K. Alam et al., Computational investigation of an unsteady non-Newtonian and non-isothermal fluid between coaxial contracting channels: A PCM approach. *Results in Physics* (2021), doi: https://doi.org/10.1016/j.rinp.2021.104570.

Computational Investigation of an unsteady Non-Newtonian and Non-Isothermal Fluid Between Coaxial Contracting Channels: A PCM Approach

Aamir Khan[a], Rehan A. Shah[b], M. Kamran Alam[a], Hijaz Ahmed[c*],
M. Shahzad[a], Sajid Rehman[b], Sohail Ahmed[d],
M. Sohail Khan[e], Abdel-Haleem Abdel-Aty[f,g], Mohammed Zakarya[h,i]

[a]Department of Pure and Applied Mathematics, The University of Haripur, KPK, Pakistan.
[b]Department of Basic Sciences and Islamiat, University of Engineering and Technology Peshawar, KPK, Pakistan.
[c]Section of Mathematics, International Telematic University Uninettuno, Corso Vittorio Emanuele II, 39,00186 Roma, Italy.
[d]Department of Mathematics, Abdul Wali Khan University Mardan, KPK, Pakistan.
[e]Department of Mathematics, Islamia College University Peshawar, KPK, Pakistan.
[f]Department of Physics, College of Sciences, University of Bisha, P.O. Box 344, Bisha 61922, Saudi Arabia.
[g]Department of Physics, Faculty of Science, Al-Azhar University, Assiut 71524, Egypt.
[h]Department of Mathematics, College of Science, King Khalid University, P.O. Box 9004, Abha 61413, Saudi Arabia.
[i]Department of Mathematics, Faculty of Science, Al-Azhar University, Assiut 71524, Egypt.

1 Abstract

The essential element of this paper is to research the porous and squeezed characteristics of time varying heats that modify the flow speed and enhance the refrigerating /boiling performance of the materials, optimize the tracers flows and minimalize instability in the non-Newtonian fluids. In the presence of no-slip velocity and convective circumstances, squeezing disks tempting laminar, unstedy and incompressible non-Newtonian fluid. The convective formulation for the equations of Navier Stokes, energy and concentration are modelled on flat disks to investigate and execute both analytical and numerical analysis of heat flow and mass transfer, which transmuted further into extremely non-linear system of ordinary differential equation with the help of similarity transformations. Regarding smears, self-similar equations with adequate starting estimates and supporting parameters are resolved by utilizing the Homotopy Analysis Method (HAM) to generate an expedited and guaranteed convergence procedure. Comparisons between HAM and the BVP4c numerical solver program demonstrate the validity and precision of HAM results. It is found by increasing or decreasing the Hartman number reduces the capillary area, making the Lorentz force influence quite visible for small non-Newtonian parameter. The concentration rate at the lower end disk rises rapidly as the thermal diffusivity rises. The radial velocity also declines because of the rise in the outflow rate from the flow domains. The suction parameter also declines. Additionally, increasing the parameter of non-Newtonian enhances the flow of temperature/mass and skin friction. In the suction / injection case, all physical factors have a reverse influence upon fluid flow patterns.

Keywords: Squeeze flow, Contracting channels, Second-grade viscoelastic fluid, Lorentz Force, HAM, BVP4c

*Corresponding Author: hijaz555@gmail.com

2 Introduction

Investigating the characteristics and distinctive qualities of non-Newtonian fluids and addressing its numerous applications, including the reduction and friction of non-Newtonian fluids, friction reduced by oil pipeline, large-scale heating and refrigeration applications, increase capacity and flow tracers, etc [1]-[10]. Expandable usage is an emergent technology with a big promises in district and building heating and cooling systems for massive energy savings. A very efficient flow tracer has been produced by combining non-Newtonian features in a color scheme. They are used to make a tracer fluid (with a coloration), which may then be unloaded as a thin strip to the turbulent flow in order to prevent dispersal and breakdown of the fluid flow. Squeeze flux is a flux type where the fluid is compressed between two parallel disks and compressed radially.
Squeezing flow is widely applied for manufacturing technology, including compression and injuction molding, blood flow caused by vessel expansion and contraction, moving pistons in engines, hydraulic brakes, lubrication, and material processing, among others. In the late 20th century, the geometry of squeezing flow attracted scientists' interest and a lot of research is being done on this. Serth was the first to produce the BVP solution given in [11][12] deprived of limiting the size of k, for the parameter of visco-elastic fluid. He saw somewhat disturbing tendency to stress upon its wall as $k's$ value grew sharply. Flow of electrically conducting non-Newtonian fluid is a very important phenomenon as in most of the practical situations we have to deal with the flow of conducting fluid which exhibits different behaviors under the influence of magnetic forces. In these cases magneto hydro dynamic (MHD) aspect of the flow is also needed to be considered. Homotopy perturbation solution for Two-dimensional MHD squeezing flow between parallel plates has been determined in [13]-[15]. To examine the generic form of second-grade fluid, in [18] Khan used laplacian and Fourier transform methods for the fluid substance. For both elastic and viscous fluid material, a fitting model is proposed to incorporate the fractional calculus method for the constitutive framework. Hayat [17] studied the oscillating flow problem in a porous half-space of an incompressible magneto hydrodynamic (MHD) second-grade fluid. To gradually evolve the solutions of sine and cosine, the Laplace transformation method is applied. Considering here that flow is symmetric at y = 0 and satisfies the no-slip condition at the top surface, approximate results are found upto 1st order. Hayat [17] also explored the detail study of oscillating fluid flow of 2nd grade incompressible magneto-hydro-dynamic (MHD) fluid in a permeable half space. To develop detailed solutions for sine and cosine oscillations, the Laplace transformation method is applied. For a 2nd grade fluid Gupta provided an analytical solution in [19] between two parallel plates using energy methods. For fixed amplitude disruptions, the stability of above flow is studied. In [20] Hayat studied the effect of 2nd grade fluid using the technique laplacian transformation. In [16], under the assumption that the magnetic field is applied perpendicularly to the fluid flow, the authors simplify the navier-stokes equations among two endless surfaces to a fourth order differential equations. The flow at y = 0 is symmetric and satisfies the no-slip condition at the top layer, approximate results are found upto 1st order. The non-Newtonian, laminar, incompressible visco-elastic fluid, time-dependent temperature and concentration between contracting disks in the polar coordinates has not been reported so far. This show that the present work on this problem to be the first such analysis in the literature. In current study, the squeezing fluid flow is time dependent between parallel disks wherein the bottom disk is porous and stationery while the above disk moves toward lower disk. The design dilemma has been resolved by HAM which proposed by Liao given in [10]. For data simulation the HAM BVPh 2.0 and BVP4c Kits are used. The residual error has been set to 10^{-40}, and the analysis are done using a 40^{th} order approximation to minimize the error and to obtain feasible outcomes.

3 Mathematical Formulation

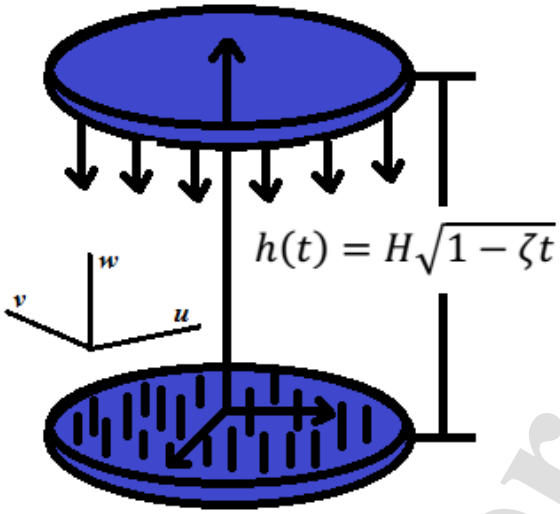

Figure 1: Geometry of the Problem.

Consider a non-Newtonian fluid between parallel disks seperated by a distance $h(t) = H(1-\zeta t)^{0.5}$, both disks are squeezed unless they meet at , $t = \zeta^{-1}$ for $+ve$ value of ζ and separated for $-ve$ value of ζ [5] . The fluid will be conducted out by electric currents with the insertion of the magnetic-field $B(t) = B_0(1-\zeta t)^{-0.5}$ and no induced-magnetic-field will be considered. The polar co-ordinate system (r, θ, z) is selected for examination of the fluid. The azimuthal component V_θ of the velocity field $\overrightarrow{U} = (V_r, V_\theta, V_z)$ is taken zero because of the absence of rotational movement of the disks i.e $\frac{\partial V_\theta}{\partial \theta} = 0$. The central point of the bottom disk is fixed as the origin with the use of cylindrical coordinates. At uniform temperatures T_l and T_u, both the top and bottom disks are preserved. The turbulent, axisymmetric, inconsistent governing equations in polar coordinates system are:

Conservation of Mass Equation [3, 4, 8]:

$$\frac{1}{r}\frac{\partial (rV_r)}{\partial r} + \frac{1}{r}\frac{\partial V_\theta}{\partial \theta} + \frac{\partial V_z}{\partial z} = 0 \tag{1}$$

Radial-component of the Momentum Equation [3, 4, 8]:

$$\frac{\partial V_r}{\partial t} + V_r\frac{\partial V_r}{\partial r} + V_\theta(\frac{1}{r}\frac{\partial V_r}{\partial \theta} - \frac{V_\theta}{r}) + V_z\frac{\partial V_r}{\partial z} = \frac{-1}{\rho}\frac{\partial p}{\partial r} + \frac{1}{\rho}\left[\frac{1}{r}\frac{\partial}{\partial r}(r\tau_{rr}) + \frac{1}{r}\frac{\partial}{\partial \theta}\tau_{r\theta} + \frac{\partial}{\partial z}\tau_{rz} - \frac{1}{r}\tau_{\theta\theta}\right] \tag{2}$$

Azimuthal-component of the Momentum Equation [3, 4, 8]:

$$\frac{\partial V_\theta}{\partial t} + V_r\frac{\partial V_\theta}{\partial r} + V_\theta(\frac{1}{r}\frac{\partial V_\theta}{\partial \theta} + \frac{V_r}{r}) + V_z\frac{\partial V_\theta}{\partial z} = -\frac{1}{r\rho}\frac{\partial p}{\partial \theta} + \frac{1}{\rho}\left[\frac{1}{r^2}\frac{\partial}{\partial r}(r^2\tau_{\theta r}) + \frac{1}{r}\frac{\partial}{\partial \theta}\tau_{\theta\theta} + \frac{\partial}{\partial z}\tau_{\theta z}\right] \tag{3}$$

Axial-component of the Momentum Equation [3, 4, 8]:

$$\frac{\partial V_z}{\partial t} + V_r\frac{\partial V_z}{\partial r} + V_\theta\frac{V_\theta}{r}\frac{\partial V_\theta}{\partial \theta} + V_z\frac{\partial V_z}{\partial z} = \frac{-1}{\rho}\frac{\partial p}{\partial z} + \frac{1}{\rho}\left[\frac{1}{r}\frac{\partial}{\partial r}(r\tau_{zr}) + \frac{1}{r}\frac{\partial}{\partial \theta}\tau_{z\theta} + \frac{\partial}{\partial z}\tau_{zz}\right] \tag{4}$$

The Energy Equation [13-15]:

$$\frac{\partial T}{\partial t} + V_r\frac{\partial T}{\partial r} + \frac{V_\theta}{r}\frac{\partial T}{\partial \theta} + V_z\frac{\partial T}{\partial z} = \frac{k}{\rho C_p}\left(\frac{\partial^2 T}{\partial r^2} + \frac{1}{r}\frac{\partial T}{\partial r} + \frac{\partial^2 T}{\partial z^2}\right) \tag{5}$$

The Transport Equation [13-15]:

$$\frac{\partial C}{\partial t}+V_r\frac{\partial C}{\partial r}+V_\theta\frac{V_\theta}{r}\frac{\partial V_\theta}{\partial \theta}+V_z\frac{\partial C}{\partial z}=D\left(\frac{\partial^2 C}{\partial r^2}+\frac{1}{r}\frac{\partial C}{\partial r}+\frac{\partial^2 C}{\partial z^2}\right) \tag{6}$$

The constitutive equation of second-grade viscoelastic fluid [22] is

$$\tau=\mu A_1+\beta_1^* A_2+\beta_2^* A_1^2 \tag{7}$$

where β_1^*, β_2^* are material constants and A_1 and A_2 are Rivlin-Ericksen tensors, such that

$$A_1=L+L^T;\ \ L=\vec{\nabla}.\vec{u}\ \ and\ \ A_2=\frac{dA_1}{dt}+A_1L+L^TA_1$$

4 Boundary Conditions

The following physical boundary conditions are considered

$$\begin{aligned} &V_r=0, \quad V_\theta=0, \quad V_z=\frac{dh}{dt}, \quad T=T_u, \quad C=C_u, \quad at \quad z=h(t)\\ &V_r=0, \quad V_\theta=0, \quad V_z=\frac{-V_{z0}}{\sqrt{1-\zeta t}}, \quad T=T_l, \quad C=C_l, \quad at \quad z=0 \end{aligned} \tag{8}$$

where τ_{ij} are the stress components, ρ is fluid density, V_r, V_θ, V_z are velocity components, similarly κ, p, C, T, C_l, C_u, T_l, T_u, D, T_m and μ are the thermal diffusivity, pressure, concentration variable, temperature variable, concentration and heat at lower and upper disks, diffusion coefficient, mean fluid temperature and dynamic viscosity of the fluid respectively.

Using the shear stress components and velocity field, the components of the Momentum equation are reduce to the following form:

Radial-component:

$$\begin{aligned} \frac{\partial V_r}{\partial t}+V_r\frac{\partial V_r}{\partial r}+V_z\frac{\partial V_r}{\partial z}=&\frac{-1}{\rho}\frac{\partial p}{\partial r}+\nu\left[\frac{\partial^2 V_r}{\partial r^2}+\frac{1}{r}\frac{\partial V_r}{\partial r}+\frac{\partial^2 V_r}{\partial z^2}+\frac{\partial^2 V_z}{\partial r\partial z}-\frac{1}{r^2}V_r\right]\\ &+\frac{\beta}{\rho}\left[2\frac{\partial V_r}{\partial z}\frac{\partial^2 V_r}{\partial z\partial r}+\frac{1}{r}(\frac{\partial V_r}{\partial z})^2+\frac{2}{r}\frac{\partial V_z}{\partial z}\frac{\partial V_r}{\partial r}+4\frac{\partial^2 V_z}{\partial z\partial r}\frac{\partial V_r}{\partial r}+2\frac{\partial V_z}{\partial z}\frac{\partial^2 V_r}{\partial r^2}\right.\\ &+\frac{2}{r}(\frac{\partial V_r}{\partial r})^2+4\frac{\partial V_r}{\partial r}\frac{\partial^2 V_r}{\partial r^2}+\frac{2}{r}\frac{\partial^2 V_r}{\partial r\partial t}+2\frac{\partial^3 V_r}{\partial r\partial t\partial r}+2\frac{\partial V_r}{\partial z}\frac{\partial^2 V_z}{\partial z^2}+2\frac{\partial^2 V_r}{\partial z^2}\frac{\partial V_z}{\partial z}\\ &+\frac{\partial^3 V_r}{\partial z\partial t\partial z}+2\frac{\partial^2 V_r}{\partial r\partial z}\frac{\partial V_z}{\partial r}-\frac{2}{r^2}\frac{\partial V_r}{\partial t}-\frac{2}{r^2}V_r\frac{\partial V_z}{\partial z}+\frac{\partial V_r}{\partial r}\frac{\partial^2 V_z}{\partial r\partial z}-2\frac{\partial V_z}{\partial r}\frac{\partial^2 V_z}{\partial r^2}\\ &\left.-\frac{2}{r^2}V_r\frac{\partial V_r}{\partial r}\right] \end{aligned} \tag{9}$$

Axial-component:

$$\begin{aligned} \frac{\partial V_z}{\partial t}+V_r\frac{\partial V_z}{\partial r}+V_z\frac{\partial V_z}{\partial z}=&\frac{-1}{\rho}\frac{\partial p}{\partial z}+\nu\left[\frac{\partial^2 V_z}{\partial r^2}+\frac{1}{r}\frac{\partial V_z}{\partial r}+\frac{\partial^2 V_r}{\partial r\partial z}+\frac{1}{r}\frac{\partial V_r}{\partial z}+\frac{\partial^2 V_z}{\partial z^2}\right]\\ &+\frac{\beta}{\rho}\left[\frac{2}{r}\frac{\partial V_r}{\partial z}\frac{\partial V_z}{\partial z}+2\frac{\partial^2 V_r}{\partial z^2}\frac{\partial V_z}{\partial z}+2\frac{\partial V_r}{\partial z}\frac{\partial^2 V_z}{\partial z\partial r}+\frac{1}{r}\frac{\partial^2 V_r}{\partial z\partial t}+\frac{\partial^3 V_r}{\partial z\partial t\partial r}\right.\\ &+\frac{2}{r}\frac{\partial V_r}{\partial r}\frac{\partial V_z}{\partial r}+2\frac{\partial^2 V_r}{\partial r^2}\frac{\partial V_z}{\partial r}+2\frac{\partial V_r}{\partial r}\frac{\partial^2 V_z}{\partial r^2}+\frac{\partial^3 V_z}{\partial r\partial t\partial r}+4\frac{\partial V_z}{\partial z}\frac{\partial^2 V_z}{\partial z^2}\\ &-2\frac{\partial V_r}{\partial z}\frac{\partial^2 V_r}{\partial z^2}+2\frac{\partial V_r}{\partial r}\frac{\partial^2 V_z}{\partial z^2}+2\frac{\partial V_z}{\partial z}\frac{\partial^2 V_r}{\partial r\partial z}+2\frac{\partial V_z}{\partial r}\frac{\partial^2 V_r}{\partial r\partial z}+2\frac{\partial V_z}{\partial r}\frac{\partial^2 V_z}{\partial r\partial z}\\ &\left.+2\frac{\partial^3 V_z}{\partial z\partial t\partial z}\right] \end{aligned} \tag{10}$$

To convert the above system of partial differential equations into a system of ordinary differential equations the similarity transformations are applied [9],

$$\begin{aligned} &V_r = \zeta r(1-\zeta t)^{-1} f'(\eta), \quad V_z = -\zeta H(1-\zeta t)^{-0.5} f(\eta), \quad \eta = zH^{-1}(1-\zeta t)^{-0.5} \\ &B(t) = B_0(1-\zeta t)^{-0.5}, \quad \theta = (T-T_u)(T_l-T_u)^{-1}, \quad \phi = (C-C_u)(C_l-C_u)^{-1} \end{aligned} \tag{11}$$

The mass conservation equation is identically satisfied and the Momentum equation, the heat equation and the mass equation are converted into the following form

$$\begin{aligned} &\frac{d^4 f}{d\eta^4} - \xi_{sq}[\eta \frac{d^3 f}{d\eta^3} + 3\frac{d^2 f}{d\eta^2} - 2f(\eta)\frac{d^3 f}{d\eta^3}] - \xi_M^2 \frac{d^2 f}{d\eta^2} + \\ &\beta[\eta \frac{d^5 f}{d\eta^5} + 6\frac{d^4 f}{d\eta^4} - 4\frac{df}{d\eta}\frac{d^4 f}{d\eta^4} - 4\frac{d^3 f}{d\eta^3}\frac{d^2 f}{d\eta^2}] = 0 \end{aligned} \tag{12}$$

$$\frac{d^2\theta}{d\eta^2} + \xi_{sq}\xi_{pr}[2f(\eta)\frac{d\theta}{d\eta} - \eta\frac{d\theta}{d\eta}] = 0 \tag{13}$$

$$\frac{d^2\phi}{d\eta^2} + \xi_{sq}\xi_L[2f(\eta)\frac{d\phi}{d\eta} - \eta\frac{d\phi}{d\eta}] = 0 \tag{14}$$

and boundary conditions are reduced to

$$\begin{aligned} &f(0) = \xi_\alpha, \quad f'(0) = 0, \quad \theta(0) = 1, \quad \phi(0) = 1 \\ &f(1) = \frac{1}{2}, \quad f'(1) = 0, \quad \theta(1) = 0, \quad \phi(1) = 0 \end{aligned} \tag{15}$$

where $\xi_M = \sqrt{\frac{\sigma B_0^2 H^2}{\nu}}$ is the Hartman number, $\xi_{sq} = \frac{\zeta H^2}{2\nu}$ is squeeze number, $\xi_\alpha = \frac{w_0}{\zeta H}$ is suction/blowing parameter, $\xi_{pr} = \frac{\nu}{\beta}$ is Prandtl number and $\xi_L = \frac{\nu}{D}$ is the Lewis number.

5 Analytic Solution by Parametric Continuation Method

Application of the parametric continuation method to the system of nonlinear equations $(12-14)$, with boundary conditions (18), and optimal choice of continuation parameter, is made in this section. The following procedural algorithm is a sequence of steps to be followed for an application of the method through matlab.

- **Canonical form of a BVP as a first order ODE**
  To convert eqs. $(12-14)$, into first order ODE, we suppose the following

$$\begin{aligned} &f = F_1, \quad f' = F_2, \quad f'' = F_3, \quad f''' = F_4 \\ &f'''' = F_5, \quad \theta = F_7, \quad \theta' = F_8 \quad \phi = F_{10}, \quad \phi' = F_{11} \end{aligned} \tag{16}$$

  Eqs. $(12-14)$, becomes

$$\eta F_5' = \frac{S_q}{\beta}\left[\eta F_4 + 3F_3 - 2F_1F_4\right] - F_4 - M^2F_3 - 6F_5 + 4F_2F_5 + 4F_4F_3 \tag{17}$$

$$F_7' = -S_q Pr\left[2F_1F_7 - \eta F_7\right] \tag{18}$$

$$F_9' = -S_q Pr\left[2F_1F_9 - \eta F_9\right] \tag{19}$$

  and the boundary conditions becomes

$$\begin{aligned} &F_1(0) = \xi_\alpha, \quad F_2(0) = 0, \quad F_6(0) = 1, \quad F_8(0) = 1, \\ &F_1(1) = 0.5, \quad F_2(1) = 0, \quad F_7(1) = 0, \quad F_9(1) = 0, \end{aligned} \tag{20}$$

- **Introduction of a parameter p and imbed obtained ODE in a p-parameter family:**
To obtain ODE in a p-parameter family, let us introduce p-parameter in eqs.$(22-26)$ and so,

$$\eta F_5' = \frac{S_q}{\beta}\left[\eta F_4 + 3F_3 - 2F_1F_4\right] - F_4 - M^2F_3 - 6(F_5-1)p + 4F_2F_5 + 4F_4F_3 \tag{21}$$

$$F_7' = -S_qPr\left[2F_1(F_7-1)p - \eta F_7\right] \tag{22}$$

$$F_9' = -S_qPr\left[2F_1(F_9-1)p - \eta F_9\right] \tag{23}$$

- **Differentiation by p, arrives at the following system with respect to sensitivities to the parametr p:**
Differentiate eqs. $(21-23)$, with respect to p

$$V_1' = A_1V_1 + R_1 \tag{24}$$

where A_1 is a coefficient matrix, R_1 is a remainder and $V_1 = \frac{dh_i}{d\tau}$, $1 \le i \le 16$.

- **Application of the supposition principle and specify Cauchy problem for each component**

$$V_1 = aU + W_1 \tag{25}$$

Here $UandW_1$ denote unknown vector functions. Solving the following two Cauchy problems for each component, we then satisfy the original ODE automatically

$$(aU + W_1)' = A_1(aU + W_1) + R_1 \tag{26}$$

and leave the boundary conditions.

- **Numerical solution of Cauchy problem**
To solve the problem, we use an implicit scheme, defined as below.

$$\frac{U^{i+1} - U^i}{\triangle\eta} = A_1U^{i+1} \tag{27}$$

$$\frac{W^{i+1} - W^i}{\triangle\eta} = A_1W^{i+1} + R_1 \tag{28}$$

- **Selection of corresponding blend coefficient**
Since, boundary conditions are applied only for h_i, where $1 \le i \le 16$. Solving ODE for sensitivities, we need to apply $V_2 = 0$, which in matrix form looks as

$$J_1.V_1 = 0 \quad \text{or} \quad J_1.(aU + W_1) = 0 \tag{29}$$

where $a = \frac{-J_1.W_1}{J_1.U}$

6 Error Analysis

To analyze the current problem, an error analysis is made by PCM and HAM BVPh 2.0 kit, with a maximum 10^{-40} residual-error is used. Analysis is performed via approximations of the 40^{th} order. To achieve the respective optimum convergence the minimize command is used. Table 1 provides the optimum values of controlling parameters and the minimum values for the over-all average residual-error according to the various orders of approximation whic show that as the order of approximation increase so as the optimal values are

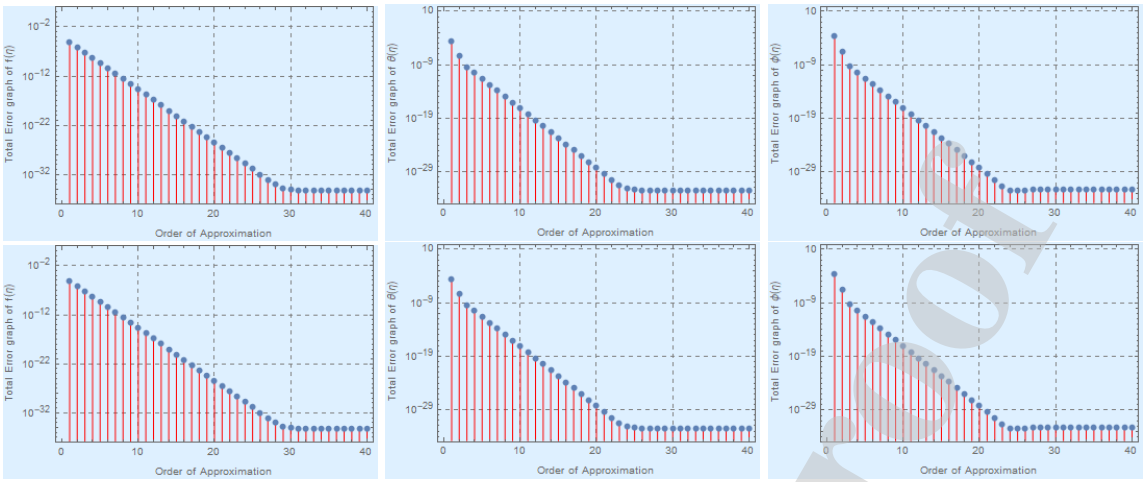

Figure 2: Average residual-error of $f(\eta), \theta(\eta)$ and $\phi(\eta)$ with different values of visco-elastic parameter $\beta = 0.01,\ 0.001$ and $\xi_{sq} = 0.01$, $\xi_{\alpha} = 2$, $\xi_M = 0.1$, $\xi_L = 1$, $\xi_{pr} = 2$

m	h^f	h_θ	h_ϕ	ϵ_m^t
2	-0.994234	-1.00354	-1.00156	5.37113×10^{-9}
3	-0.992433	-1.00048	-1.00013	3.23957×10^{-13}
4	-0.993395	-0.997935	-0.995064	-1.48837×10^{-15}
5	-0.970283	-0.981944	-1.036390	4.01980×10^{-14}
6	-1.06583	-1.075180	-0.942538	-6.19490×10^{-15}

Table 1: Different order of approximation versus optimal values of convergence control parameters at $\xi_{sq} = 0.01, \xi_{\alpha} = 2, \xi_M = 0.1, \xi_L = 1, \xi_{pr} = 2, \beta = 0.001$.

getting close to 1.Table 2 demonstrates the specific average residual-error at various orders of approximations utilizing the optimum outputs of Table 1. Moreover, the errors curves for the various values of m and fixed values of $\xi_M, \xi_L, \xi_{\alpha}, \xi_{pr}$ and ξ_{sq} are exposed in Fig 2. It is apparent because, as the approximation order rises, the average squared-errors and the overall average squared-errors are reduced. Authentications of boundary conditions is shown through Table 3. Through this study, it would seem that the results are nearly in the 10^{th} order of approximations. For further validation we add the numerical results of $f''(0)$, $-\theta'(0)$ and $-\phi'(0)$ in Table $(4-6)$ which shows that the convergence is up to tenth-order. Convergence of Homotopy solution for different orders of approximation for $f''(0)$, $-\theta'(0)$ and $-\phi'(0)$ when $\xi_{sq} = 0.01$, $\xi_M = 0.1$, $\xi_{pr} = 2$, $\xi_L = 1$, $\xi_{\alpha} = 2$ and different values of $\beta = 0.001, 0.01, 0.05$ are depicted in Tables $(4-6)$. It is observed that by increase in the visco-elastic parameter, the skin-friction, heat and mass fluxes are also increases. The effects of physical parameters on the skin friction, heat flux and mass flux are also studied and depicted in Tables $(7-9)$.

m	${\epsilon^f}_m$	${\epsilon^\theta}_m$	${\epsilon^\phi}_m$	$CPUtime$
2	3.5×10^{-6}	4.7×10^{-10}	1.1×10^{-8}	2 sec
5	2.8×10^{-17}	4.8×10^{-18}	4.3×10^{-176}	8.5 sec
10	3.7×10^{-24}	3.2×10^{-25}	1.1×10^{-22}	15.3 sec
15	4.4×10^{-30}	3.2×10^{-33}	3.3×10^{-30}	30.6 sec
20	3.9×10^{-35}	2.1×10^{-36}	6.3×10^{-34}	46.8 sec
25	3.1×10^{-35}	2.3×10^{-36}	5.8×10^{-34}	80.4 sec
30	3.1×10^{-35}	1.9×10^{-36}	5.9×10^{-34}	123.5 sec
35	3.1×10^{-35}	1.7×10^{-36}	5.8×10^{-34}	270.3 sec
40	3.1×10^{-35}	1.9×10^{-36}	6.7×10^{-34}	401.4 sec

Table 2: Total Residual Error at different order of approximation at $\xi_{sq} = 0.01$, $\xi_M = 0.1$, $\xi_{pr} = 2$, $\beta = 0.001$, $\xi_L = 1$ and $\xi_\alpha = 2$

η	HAM			BVP4c			PCM		
	$f(\eta)$	$\theta(\eta)$	$\phi(\eta)$	$f(\eta)$	$\theta(\eta)$	$\phi(\eta)$	$f(\eta)$	$\theta(\eta)$	$\phi(\eta)$
0	2	1	1	2	1	1	2	1	1
0.1001	0.014101	0.899947	0.899520	0.014101	0.899947	0.899518	0.014295	0.899019	0.899581
0.3003	0.108528	0.699840	0.698602	0.108528	0.699838	0.698602	0.108677	0.699961	0.698611
0.5005	0.250757	0.499701	0.497915	0.250757	0.499700	0.497914	0.250899	0.499823	0.497929
0.7007	0.392641	0.297737	0.297737	0.392641	0.29772	0.297736	0.392345	0.297855	0.297756
0.8008	0.448480	0.197930	0.197930	0.448480	0.197930	0.197927	0.448519	0.197920	0.197920
0.9009	0.486265	0.098346	0.098346	0.486266	0.098346	0.098345	0.486300	0.098357	0.098464
1	0.5	0	0	0.5	0	0	0.5	0	0

Table 3: HAM, BVP4c and PCM results comparison of $f(\eta)$, $\theta(\eta)$ and $\phi(\eta)$ at $\xi_{sq} = 0.01, \xi_\alpha = 2, \xi_M = 0.1, \xi_L = 1, \xi_{pr} = 2, \beta = 0.001$.

m	$f''(0)$	$-\theta'(0)$	$-\phi'(0)$
4	−9.05372854	1.02760954	1.01376504
8	−9.05374433	1.02796615	1.01390527
12	−9.05374433	1.02796615	1.01390527
16	−9.05374433	1.02796615	1.01390527
20	−9.05374433	1.02796615	1.01390527
24	−9.05374433	1.02796615	1.01390527
28	−9.05374433	1.02796615	1.01390527
32	−9.05374433	1.02796615	1.01390527
36	−9.05374433	1.02796615	1.01390527
40	−9.05374433	1.02796615	1.01390527

Table 4: HAM solution for different orders of approximation for $f''(0)$, $-\theta'(0)$ and $-\phi'(0)$ at $\xi_{sq} = 0.01$, $\xi_M = 0.1$, $\xi_{pr} = 2$, $\beta = 0.001$, $\xi_L = 1$ and $\xi_\alpha = 2$

m	$f''(0)$	$-\theta'(0)$	$-\phi'(0)$
4	−9.03829731	1.15231781	1.14532672
8	−9.03835429	1.15251239	1.14571876
12	−9.03835429	1.15251239	1.14571876
16	−9.03835429	1.15251239	1.14571876
20	−9.03835429	1.15251239	1.14571876
24	−9.03835429	1.15251239	1.14571876
28	−9.03835429	1.15251239	1.14571876
32	−9.03835429	1.15251239	1.14571876
36	−9.03835429	1.15251239	1.14571876
40	−9.03835429	1.15251239	1.14571876

Table 5: HAM solution for different orders of approximation for $f''(0)$, $-\theta'(0)$ and $-\phi'(0)$ at $\xi_{sq} = 0.01$, $\xi_M = 0.1$, $\xi_{pr} = 2$, $\beta = 0.01$, $\xi_L = 1$ and $\xi_\alpha = 2$

7 Results and Discussions

To explore and investigate the impacts of porosity and squeezing phenomena in the presence of fluctuating temperature on flow rate, optimise the system's heating/cooling process, reduce non-Newtonian fluid turbulence, and scale-up flow tracers. By using non-Newtonian flow created by compressing discs, which is laminar, unstable, and incompressible in the presence of no-slip velocity and convective surface boundary conditions, to investigate and provides an analytical and numerical study of the flow for heat and mass transfer. The effect of the various flow parameters are addressed visually for the case of suction ($\xi_\alpha < 0$) and injection ($\xi_\alpha > 0$) respectively. The effect of the flow parameters is shown for the axial $f(\eta)$ and radial $f'(\eta)$ components of velocity field, variation of temperature $\theta(\eta)$ and for the variation of mass transfer $\phi(\eta)$ respectively. In this section the impact of injection/suction parameter ξ_α, squeeze Reynold number ξ_{sq}, Prandtl number ξ_{pr}, Lewis number ξ_L, Hartman number ξ_M and non-Newtonian parameter β respectively are analyzed and discussed in detail. If ξ_{sq} is $+ve$, it shows the top of the disk moves far from the bottom disk and when ξ_{sq} is $-ve$, it shows the top of the disk moves close to the bottom disk. However, it is visible that an increment in ξ_{sq} can be viewed as an increase over the top disk velocity or in the gap among the two-discs [12-15].

Standard findings for the injection/suction parameter ξ_α are presented in figures $(3-10)$ to explore its effect

m	$f''(0)$	$-\theta'(0)$	$-\phi'(0)$
4	−9.00956247	1.38725923	1.45889274
8	−9.00998752	1.38776257	1.45899982
12	−9.00998752	1.38776257	1.45899982
16	−9.00998752	1.38776257	1.45899982
20	−9.00998752	1.38776257	1.45899982
24	−9.00998752	1.38776257	1.45899982
28	−9.00998752	1.38776257	1.45899982
32	−9.00998752	1.38776257	1.45899982
36	−9.00998752	1.38776257	1.45899982
40	−9.00998752	1.38776257	1.45899982

Table 6: HAM solution for different orders of approximation for $f''(0)$, $-\theta'(0)$ and $-\phi'(0)$ at $\xi_{sq} = 0.01$, $\xi_M = 0.1$, $\xi_{pr} = 2$, $\beta = 0.05$, $\xi_L = 1$ and $\xi_\alpha = 2$

P_r	HAM			BVP4c			PCM		
	$f''(0)$	$-\theta'(0)$	$-\phi'(0)$	$f''(0)$	$-\theta'(0)$	$-\phi'(0)$	$f''(0)$	$-\theta'(0)$	$-\phi'(0)$
0.1	3.404551	0.980413	1.153067	3.404550	0.980413	1.153067	3.404633	0.980592	1.153196
1	3.404551	0.918726	1.159177	3.404550	0.918726	1.159177	3.404611	0.918870	1.159203
2	3.404551	0.844146	1.166561	3.404550	0.844141	1.166563	3.404633	0.844294	1.166622
2.5	3.404551	0.804209	1.170511	3.404550	0.804192	1.170517	3.404633	0.804359	1.170691
3	3.404551	0.763560	1.173853	3.404550	0.762300	1.174664	3.404646	0.763601	1.173981

Table 7: HAM, BVP4c and PCM result comparison for the computations of $f''(0)$, $-\theta'(0)$ and $-\phi'(0)$ at $\beta = 0.1$, $\xi_M = 1$, $\xi_L = 2$, $\xi_\alpha = 2$, $\xi_{sq} = 0.2$ and different values of ξ_{pr}.

on the velocity field components, heat, and mass transfers. It is evident from figure 3 that an increase in the suction/injection parameter $\xi_\alpha = -5, -10, -15$ decreases the radial velocity due to the increase in the rate of outflow from the flow domain. On the other hand, an increase in the injection parameter $\xi_\alpha = 5, 10, 15$ allows the fluid to enter the flow domain which increases the radial velocity near the lower disk. It can also be observed that by rising the non-Newtonian parameter $\beta = 0.2, 0.4, 0.6, 0.8$, parabolic curves are found for both suction and injection. Figure 4 is made to depict the $3D$-behavior of the effect of ξ_α and β on the radial component of the velocity field. The physics of the figure 3 implies that the increase in the suction/injection parameter will increase the axial velocity due to the suction of the fluid from the lower disk, same but opposite behavior is noted during injection of the fluid between the gap of the two disks. This phenomenon could be verified from figures 5 and 6. The influence of ξ_α on heat and mass transfer is depicted in figures $(7 - 10)$. Firstly, the effect of suction and injection parameter on $\theta(\eta)$ and $\phi(\eta)$ are observed identical. Secondly the variation for higher values are smooth in $\phi(\eta)$ and $\theta(\eta)$. An increase in the rate of suction $\xi_\alpha = 0.5, 1, 1.5$ increases the rate of outflow from the flow domain due to which the fluid temperature and mass transfer fall. The same but opposite behavior is noted in the case of fluid injection. Figure 8 and 10 are drawn to observe this phenomenon in $3D$ shape.

The impact of ξ_M and β on $f'(\eta)$ and $f(\eta)$ are seen at figures $(11 - 14)$. Hartmann number is the ratio of electromagnetic force to viscous force, by increasing ξ_M and skipping Hartman number a vascular area is noted. It could be observed that during the injection of the fluid, radial velocity increase near the two disks due to the decrease in the viscous force. This phenomenon is opposite near the center of the fluid domain. The impact of ξ_M during the suction of the fluid is negligible, It also describes that Lorentz-force has a smoother

ξ_{sq}	HAM			BVP4c			PCM		
	$f''(0)$	$-\theta'(0)$	$-\phi'(0)$	$f''(0)$	$-\Theta'(0)$	$-\phi'(0)$	$f''(0)$	$-\theta'(0)$	$-\phi'(0)$
0.1	5.731321	0.998768	1.009664	5.731321	0.998768	1.009664	5.731461	0.998867	1.009751
1	3.425398	0.990088	1.077669	3.425399	0.990088	1.077668	3.425480	0.990196	1.077798
2	3.404551	0.980413	1.153067	3.404550	0.980413	1.153067	3.404699	0.980525	1.153191
3	3.474725	0.970731	1.227853	3.474725	0.970730	1.227853	3.474859	0.970825	1.227862
4	3.565737	0.961063	1.301666	3.565737	0.961063	1.301666	3.565844	0.961124	1.301731

Table 8: HAM, BVP4c and PCM results comparison for the computations of $f''(0)$, $-g'(0)$, $-\Theta'(0)$ and $-\phi'(0)$ at $\beta = 0.1$, $\xi_M = 1$, $\xi_L = 2$, $\xi_\alpha = 2$, $\xi_{pr} = 2$ and different values of ξ_{sq}.

ξ_L	HAM			BVP4c			PCM		
	$f''(0)$	$-\theta'(0)$	$-\phi'(0)$	$f''(0)$	$-\theta'(0)$	$-\phi'(0)$	$f''(0)$	$-\theta'(0)$	$-\phi'(0)$
1	4.354185	0.999448	1.004323	4.354185	0.999448	1.004323	4.354273	0.999357	1.004401
2	8.388572	0.999249	1.005891	8.388587	0.999249	1.005891	8.388629	0.999361	1.005925
3	15.08649	0.998920	1.008476	15.08649	0.998920	1.008476	15.08653	0.998041	1.008525
4	24.40871	0.998467	1.012038	24.40871	0.998467	1.012038	24.40944	0.998585	1.012136
5	36.30043	0.997897	1.016526	36.30045	0.997897	1.016526	36.30191	0.997937	1.016692

Table 9: HAM, BVP4c and PCM results comparison for the computations of $f''(0)$, $-\theta'(0)$ and $-\phi'(0)$ at $\beta = 0.1$, $\xi_M = 1$, $\xi_{sq} = 2$, $\xi_\alpha = 2$, $\xi_{pr} = 1$ and different values of ξ_L.

effect on $\beta = 0.2, 0.4\, 0.6$, 0.8 and greater values. For the axial velocity, the velocity increase near the lower disk because of the injection of the fluid which mobilizes the fluid to move in the axial direction. This effect gradually decreases due to a decrease in the viscous force and hence from the middle region, the velocity starts to decrease. Figures 12 and 14 are made to observe the effect of ξ_M in $3D$ geometries. Figures 15 and 16 present the impact of the Prandtl number on the heat transfer. Prandtl number is the ratio of momentum diffusivity to thermal diffusivity. Figure 15 explains the impact of Prandtl number ξ_{pr} on temperature. It is noted that while in suction, the flow temperature increases with an increase in the amount of Prandtl and the visco-elastic parameter because of the increase in momentum diffusivity, although this behavior is inversely proportional during injection of the fluid between the disks. For variable β and ξ_{sq} figures $(16-23)$ are plotted. The profiles of velocity components plotted in figure 16 show that initially, the redial part of the velocity rises with the increase of ξ_{sq} when the fluid is injected, but, as the fluid flow reached the central area it gradually falls. The maximal decrements for the lower values of ξ_{sq} can be observed on the radial-velocity. Velocity increases with the increase in ξ_{sq} on the left of the bottom disk, whereas velocity decreases for the same ξ_{sq} upon the right of the top disk. Furthermore, the squeeze-parameter effect is not visible for the large β, but for tiny β is noticeable as the top of the disk is heading away from the bottom disk. In figure 16 also demonstrate that velocity changes are negligible by increasing space between disks during injection of the fluid. In a suction scenario, it would be noticeable that the effects of $f'(\eta)$ are relatively greater when β is small. It may also be observed that for small squeezing parameters, $f'(\eta)$ abruptly rises close to the bottom disk afterward begins to decrease to meet boundary conditions. The effect of $\xi_{sq} = -0.1, -1, -1$ on axial velocity profile could also be seen its graphical representation in figure 18. The minor impact of ξ_{sq} observed on the velocity profile for the minimal amount of β but for larger β this effect is negligible. The effect of suction on velocity is the opposite of injection. Figures 20 depicts that as the fluid slips from the disk's region the temperature of the fluid decrease abruptly due to suction, however, this behavior is the opposite in the case of injection. A similar scenario could be seen for the mass transfer in figure 22.

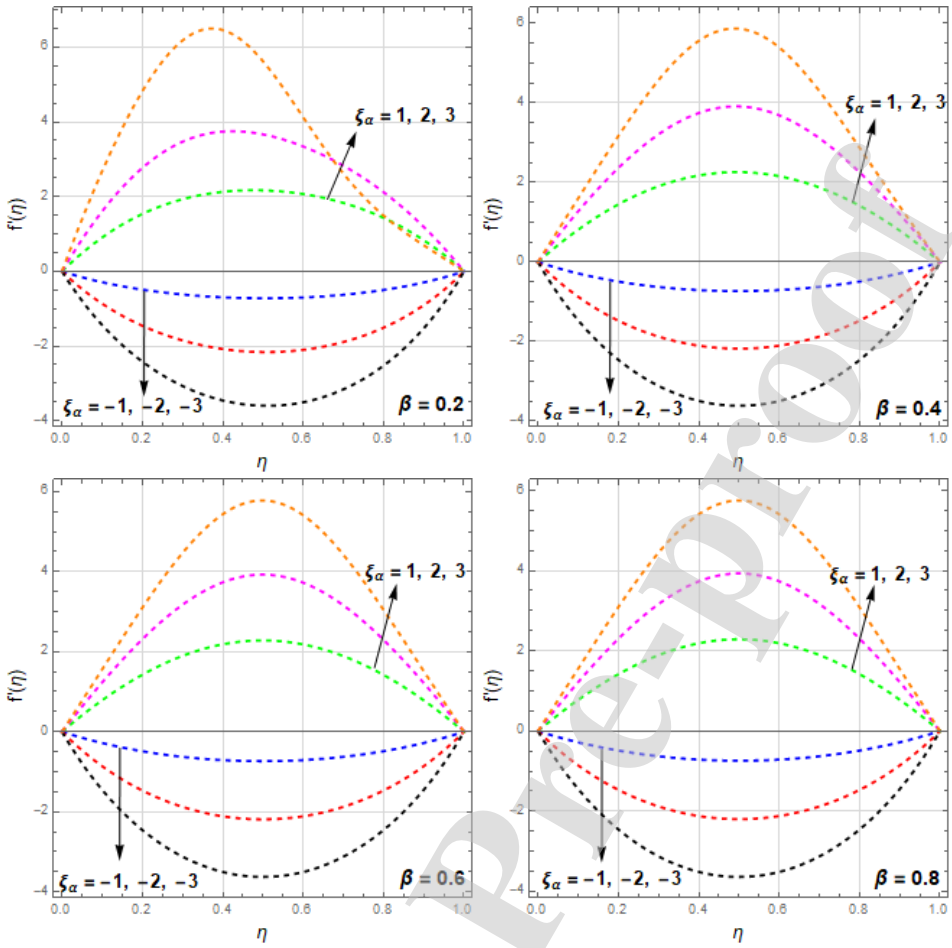

Figure 3: Impact of suction/Injection parameter $\xi_\alpha = \pm 5, \pm 10, \pm 15$ and $\beta = 0.2, 0.4, 0.6, 0.8$ on $f'(\eta)$ with $\xi_{sq} = 5$, $\xi_M = 10$, $\xi_{pr} = 1$, $\xi_L = 1.5$

The impact of Lewis number is presented in figures 24 and 25. Lewis number is the ratio of thermal diffusivity to mass diffusivity. An increase in the Lewis number means an increase in the thermal diffusivity of the fluid. It Could be observed that for greater Lewis number, $\phi(\eta)$ abruptly falls close to the bottom disk afterward begins to decrease to meet boundary conditions. The minor impact of ξ_L was observed on the concentration profile for the minimal amount of β but for larger β this effect is negligible. Figure 25 presents the $3D$ view of the effect of Lewis number on mass transfer.

8 Conclusion

In this research Non-Newtonian fluid is examined as a turbulent squeezing flow amongst two parallel discs. Using the Parametric Continuation Method (PCM) and BVP4c for the numerical solution to solve the derived differential equations given in equations (13-15). At just 10th-order analytical solution, a good averaged residual error is produced. During the analysis, the following results were achieved. In the case of suction and injection, the effect of different flow parameters are examined visually. For velocity field, heat, and mass transfer, the influence of the flow parameters is presented. During this study, the results obtained are:

- The current problem is limited to two-dimensional geometry, which can be changed to three-dimensional

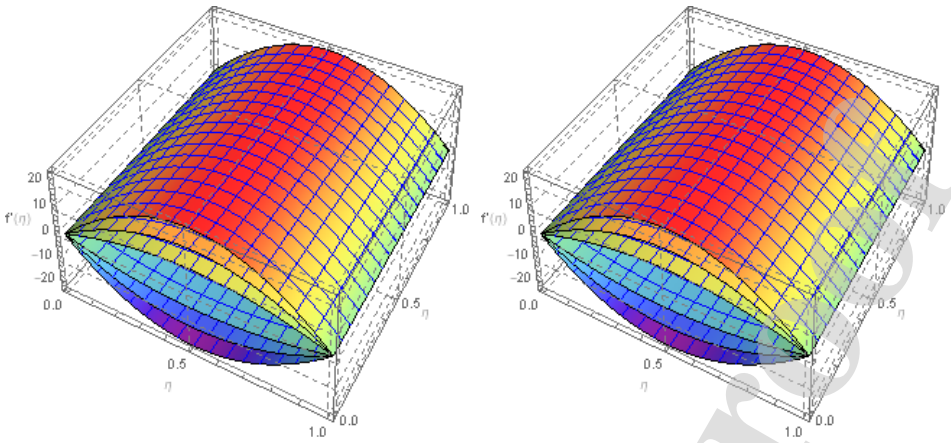

Figure 4: 3D-representation of $f'(\eta)$ for $\xi_\alpha = \pm 5, \pm 10, \pm 15$, $\beta = 0.6, 0.8$, $\xi_{sq} = 5$, $\xi_M = 10$, $\xi_{pr} = 1$, $\xi_L = 1.5$

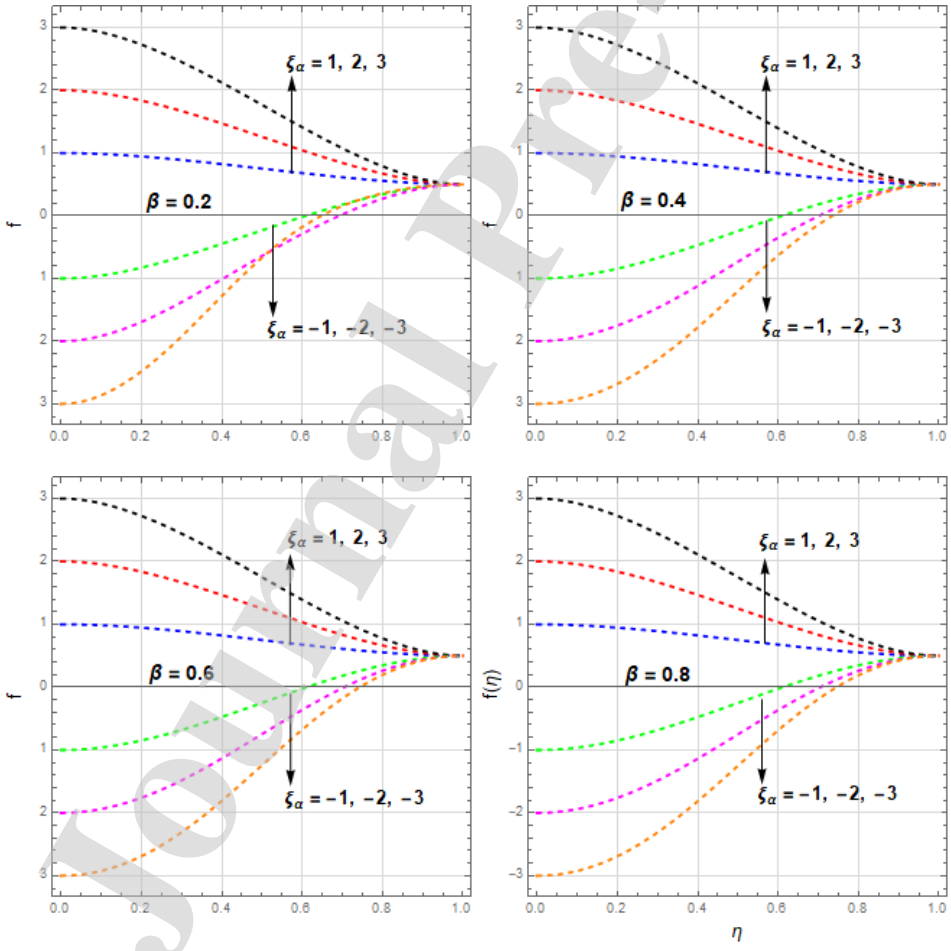

Figure 5: Impact of suction/Injection parameter $\xi_\alpha = \pm 5, \pm 10, \pm 15$ and $\beta = 0.2, 0.4, 0.6, 0.8$ on $f(\eta)$ with $\xi_{sq} = 5$, $\xi_M = 10$, $\xi_{pr} = 1$, $\xi_L = 1.5$

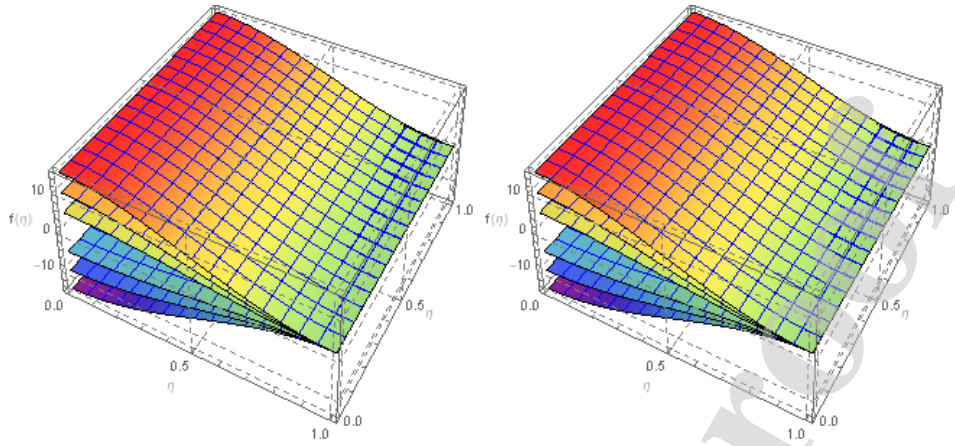

Figure 6: 3D-representation of $f(\eta)$ for $\xi_\alpha = \pm 5, \pm 10, \pm 15$, $\beta = 0.6, 0.8$, $\xi_{sq} = 5$, $\xi_M = 10$, $\xi_{pr} = 1$, $\xi_L = 1.5$

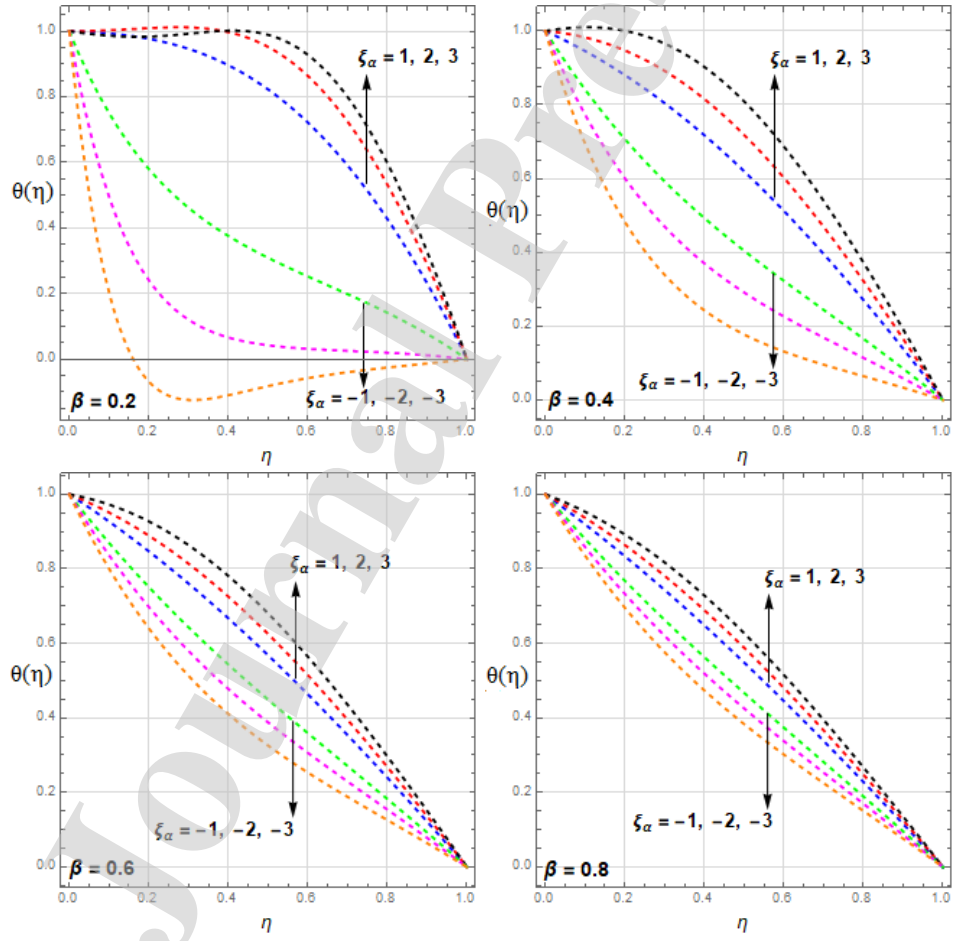

Figure 7: Impact of suction/Injection parameter $\xi_\alpha = \pm 0.5, \pm 1, \pm 1.5$ on $\theta(\eta)$ with $\beta = 0.2, 0.4, 0.6, 0.8$ and $\xi_{sq} = 1$, $\xi_M = 5$, $\xi_{pr} = 1$, $\xi_L = 1.5$

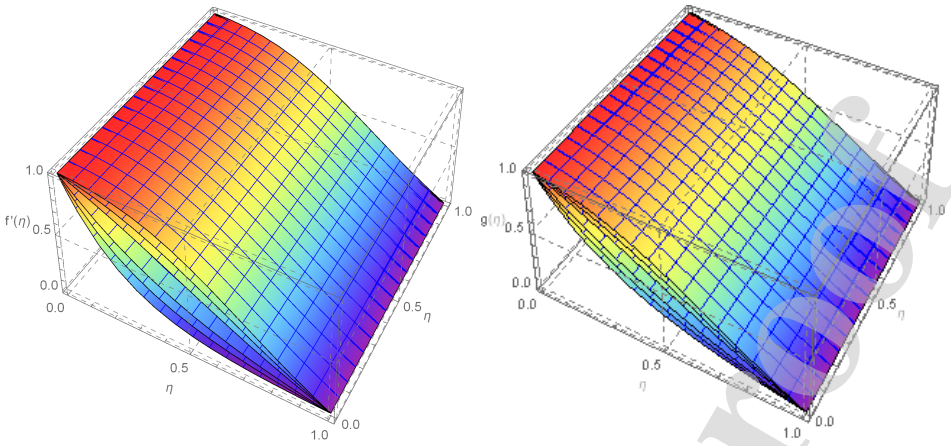

Figure 8: 3D-representation of $\theta(\eta)$ with $\xi_\alpha = \pm 0.5, \pm 1, \pm 1.5$, $\beta = 0.6, 0.8$, $\xi_{sq} = 1$, $\xi_M = 5$, $\xi_{pr} = 1$, $\xi_L = 1.5$

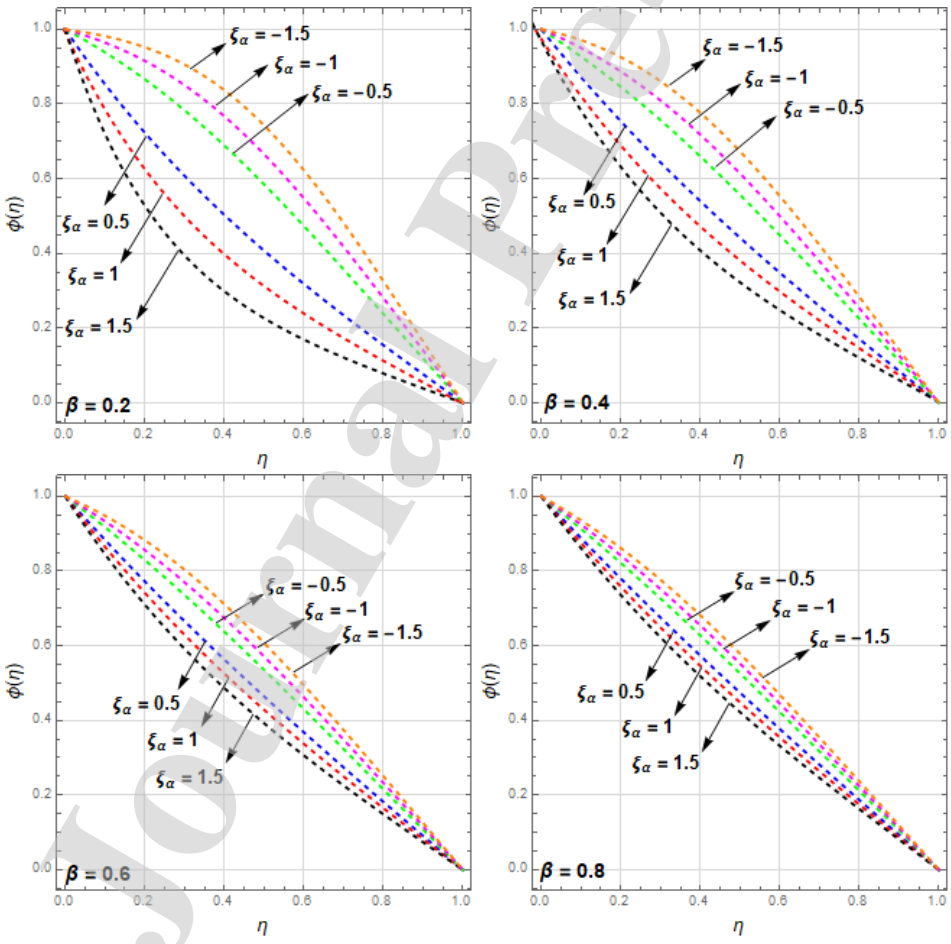

Figure 9: Impact of suction/Injection parameter $\xi_\alpha = \pm 0.5, \pm 1, \pm 1.5$ on $\phi(\eta)$ with $\beta = 0.2, 0.4, 0.6, 0.8$ and $\xi_{sq} = 1$, $\xi_M = 5$, $\xi_{pr} = 1$, $\xi_L = 1.5$

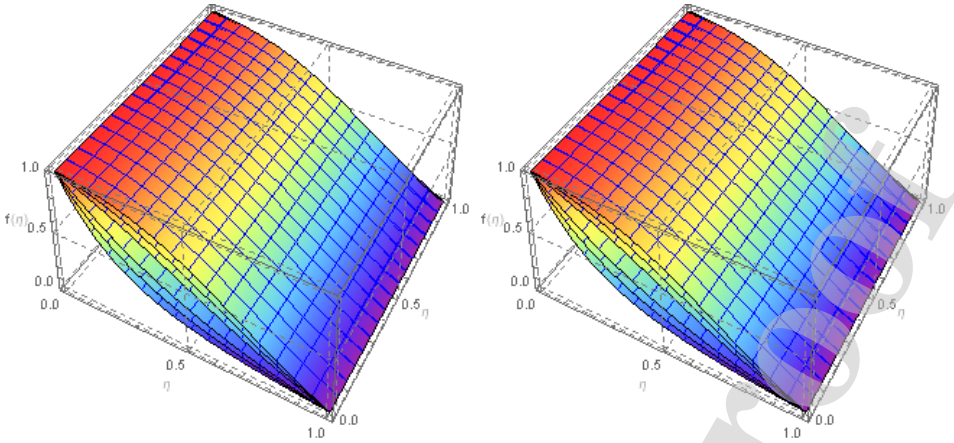

Figure 10: 3D-representation of $\phi(\eta)$ with $\xi_\alpha = \pm 0.5, \pm 1, \pm 1.5$, $\beta = 0.2, 0.4, 0.6, 0.8$, $\xi_{sq} = 1$, $\xi_M = 5$, $\xi_{pr} = 1$, $\xi_L = 1.5$

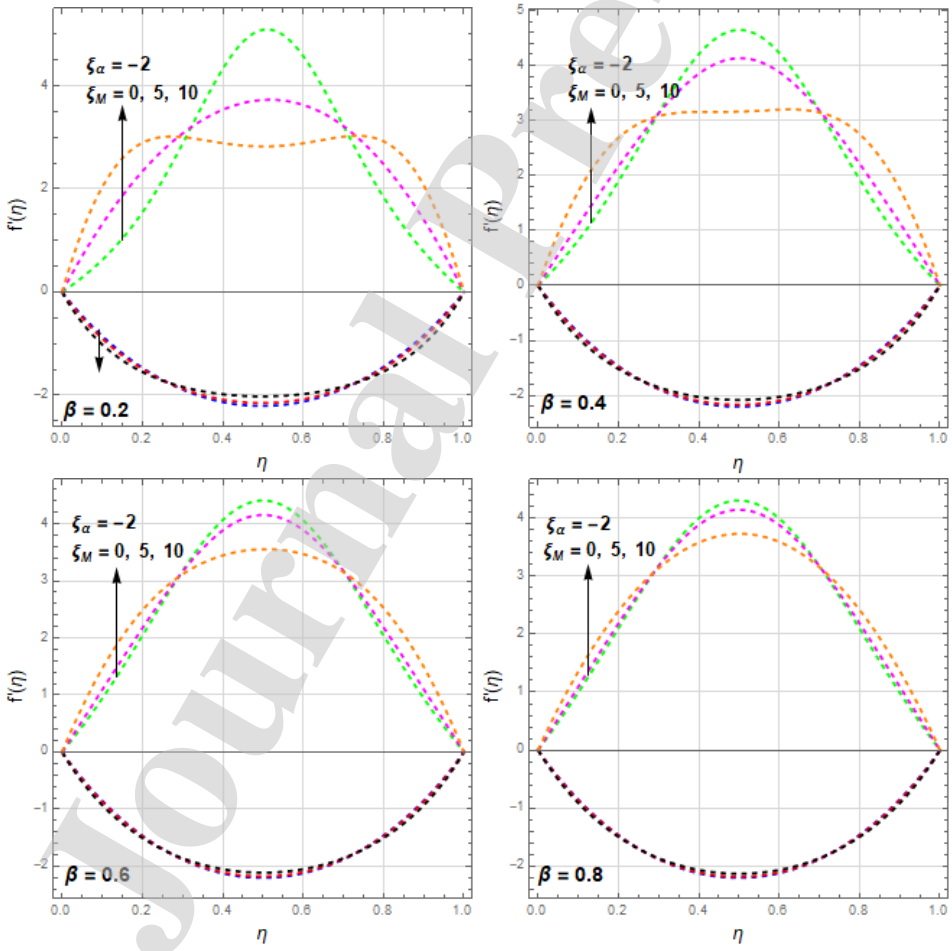

Figure 11: Impact of Hartmann number $\xi_M = 0,\ 5,\ 10$ and $\beta = 0.2, 0.4, 0.6, 0.8$ on $f'(\eta)$ with $\xi_{sq} = 0.1$, $\xi_{pr} = 5$, $\xi_L = 1$, $\xi_\alpha = \pm 2$

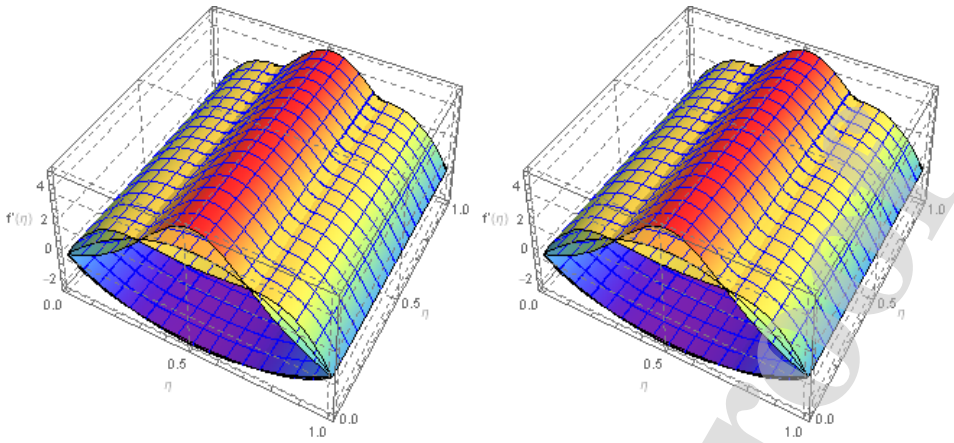

Figure 12: 3D-representation of Hartmann number $\xi_M = 0, 5, 10$ and $\beta = 0.2, 0.4, 0.6, 0.8$ on $f'(\eta)$ with $\xi_{sq} = 0.1$, $\xi_{pr} = 5$, $\xi_L = 1$, $\xi_\alpha = \pm 2$

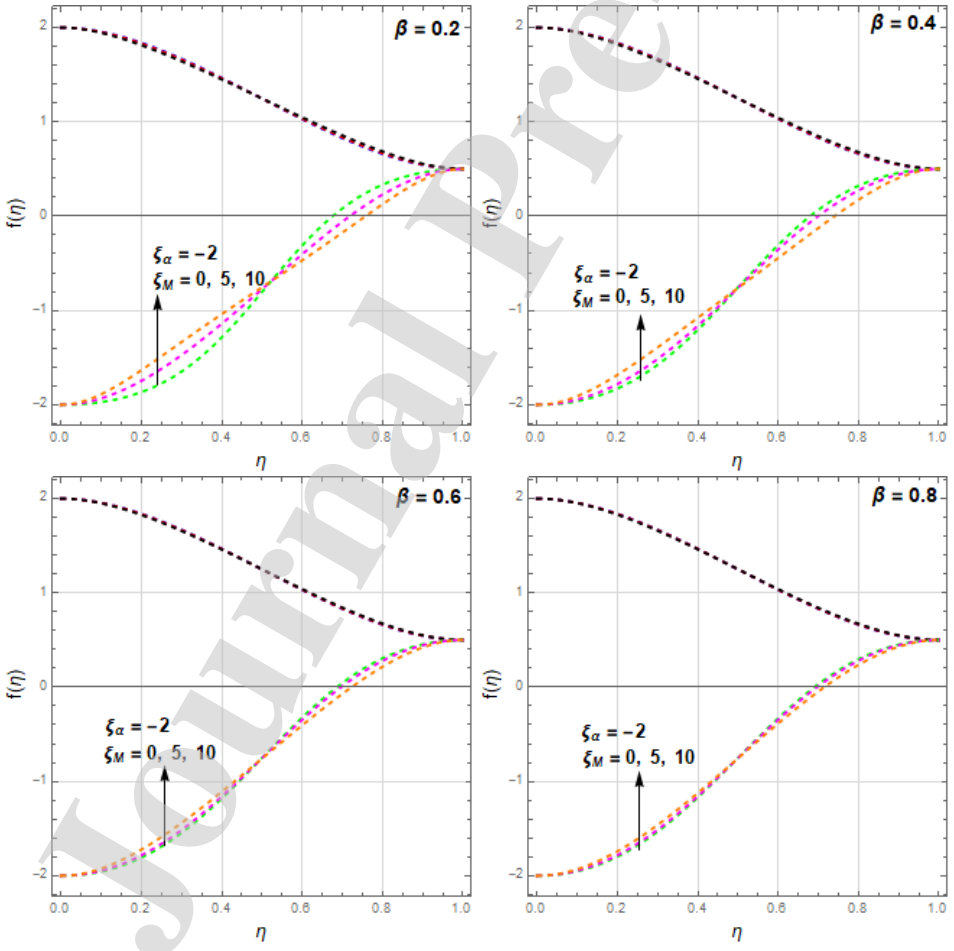

Figure 13: Impact of Hartmann number $\xi_M = 0, 5, 10$ and $\beta = 0.2, 0.4, 0.6, 0.8$ on $f(\eta)$ with $\xi_{sq} = 0.1$, $\xi_{pr} = 5$, $\xi_L = 1$, $\xi_\alpha = \pm 2$

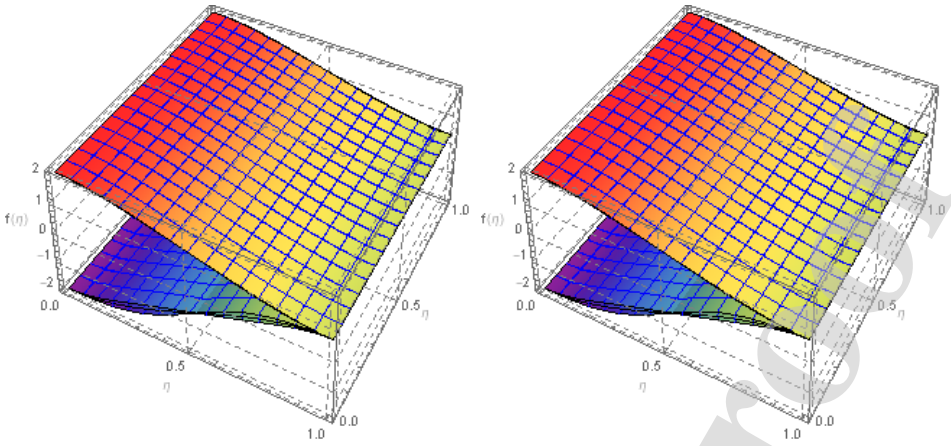

Figure 14: 3D-representation of Hartmann number $\xi_M = 0,\ 5,\ 10$ and $\beta = 0.2, 0.4, 0.6, 0.8$ on $f(\eta)$ with $\xi_{sq} = 0.1$, $\xi_{pr} = 5$, $\xi_L = 1$, $\xi_\alpha = \pm 2$

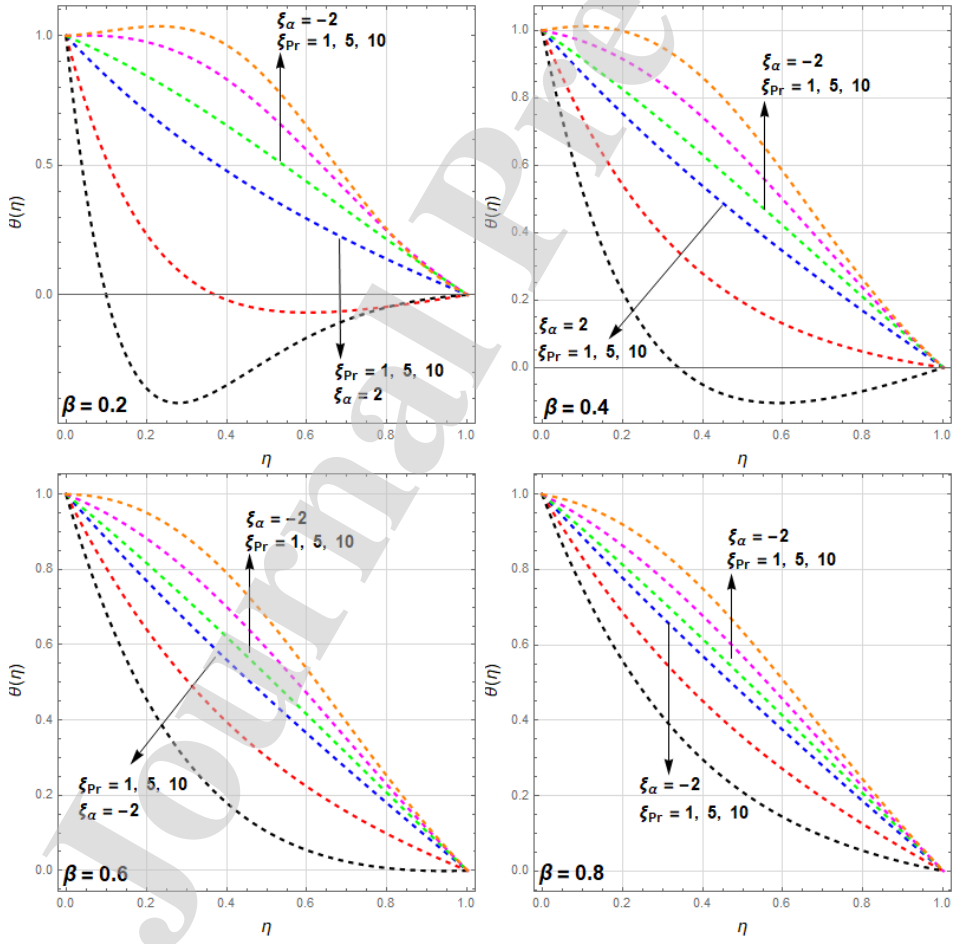

Figure 15: Impact of Prandtl number $\xi_{pr} = 1,\ 5,\ 10$ and $\beta = 0.2, 0.4, 0.6, 0.8$ on $\theta(\eta)$ with $\xi_{sq} = 0.1$, $\xi_M = 5$, $\xi_L = 1$, $\xi_\alpha = \pm 2$

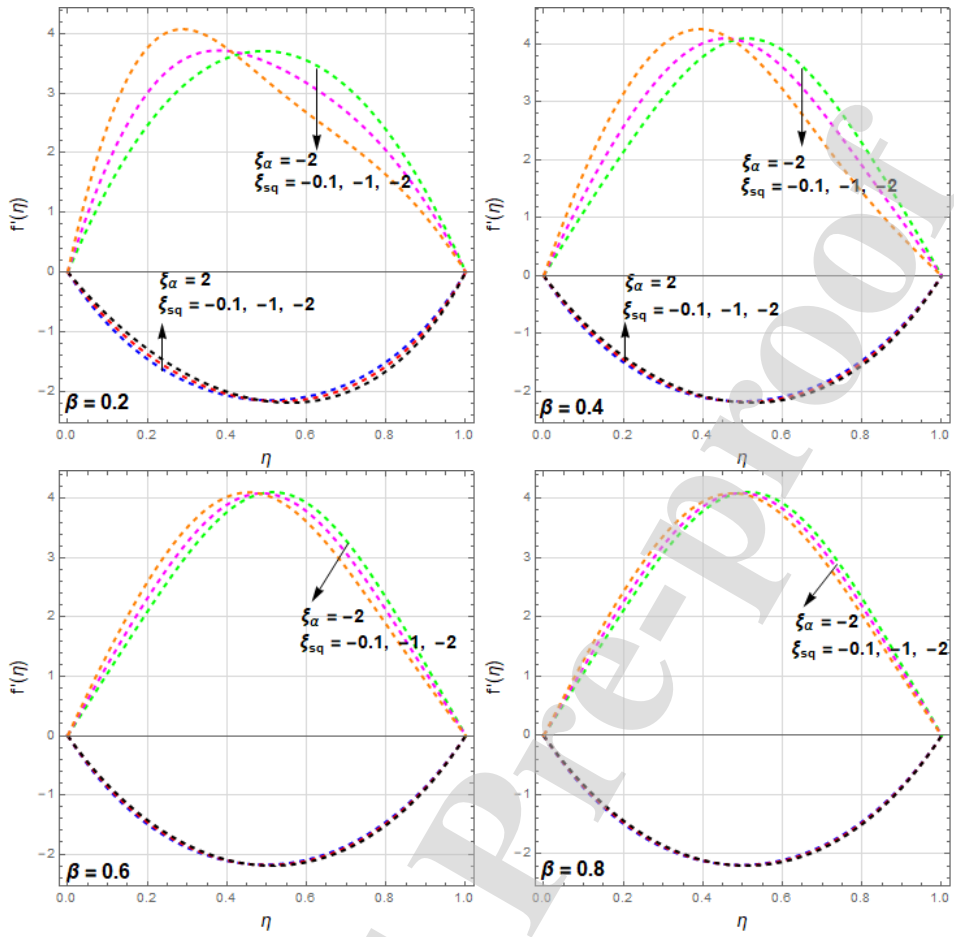

Figure 16: Impact of squeezing parameter $\xi_{sq} = -0.1, -1, -2$ with $\beta = 0.2, 0.4, 0.6, 0.8$ on $f'(\eta)$ and $\xi_M = 5$, $\xi_{pr} = 2$, $\xi_L = 1$, $\xi_\alpha = \pm 2$

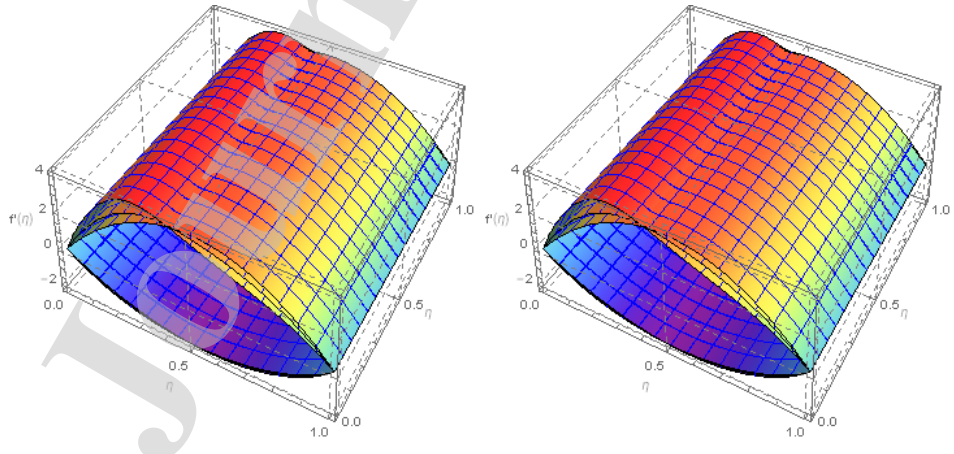

Figure 17: 3D-representation of squeezing parameter $\xi_{sq} = -0.1, -1, -2$ and $\beta = 0.2, 0.4, 0.6, 0.8$ on $f'(\eta)$ with $\xi_M = 5$, $\xi_{pr} = 2$, $\xi_L = 1$, $\xi_\alpha = \pm 2$

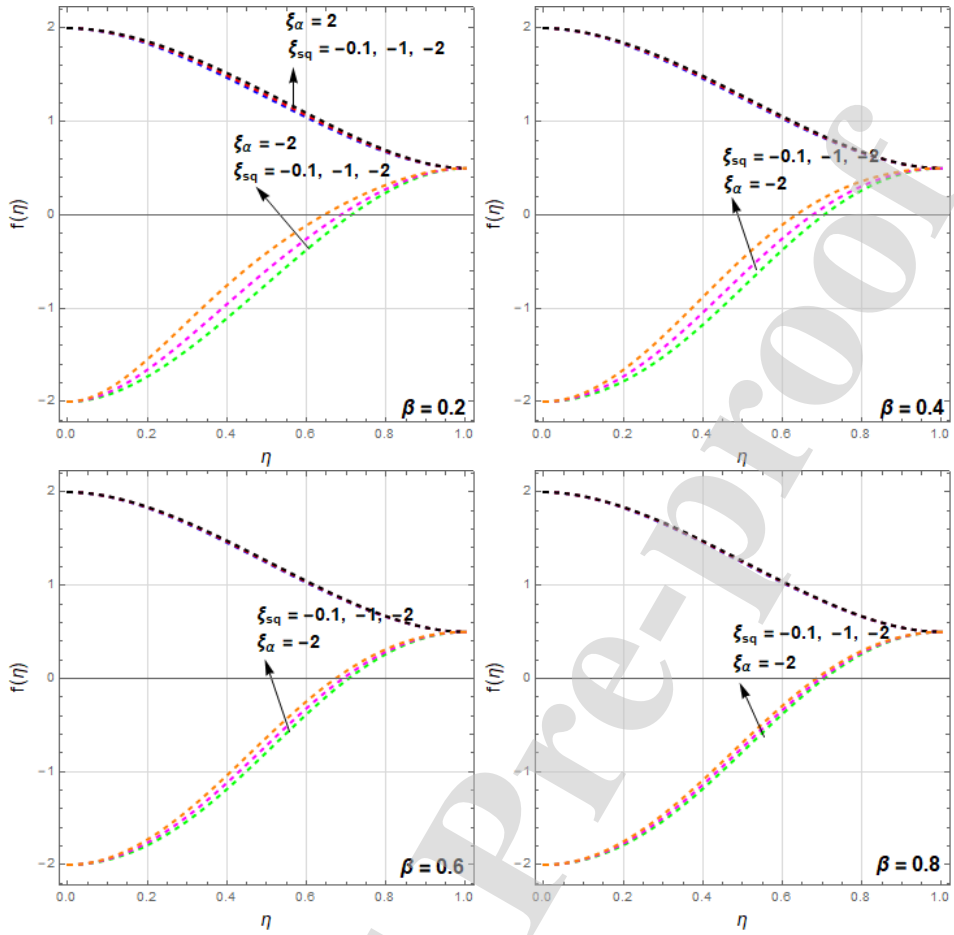

Figure 18: Impact of squeezing parameter $\xi_{sq} = -0.1, -1, -2$ and $\beta = 0.2, 0.4, 0.6, 0.8$ on $f(\eta)$ with $\xi_M = 5$, $\xi_{pr} = 2$, $\xi_L = 1$, $\xi_\alpha = \pm 2$

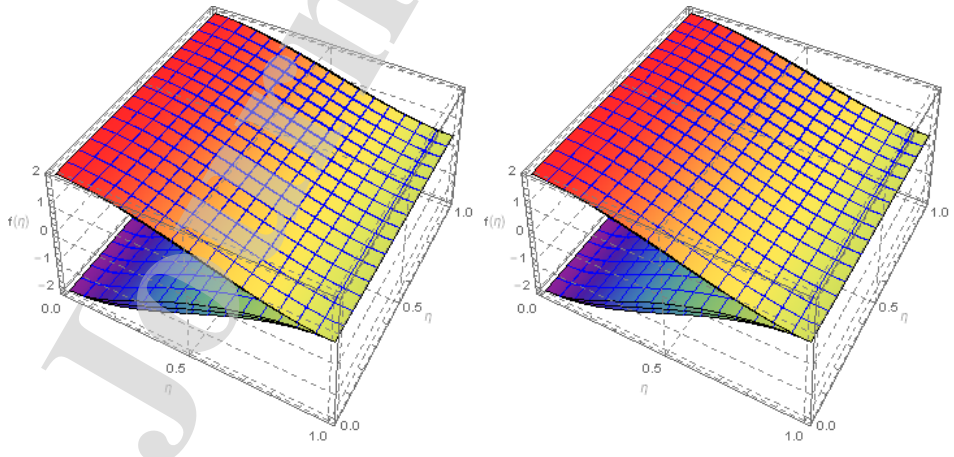

Figure 19: 3D-representation of squeezing parameter $\xi_{sq} = -0.1, -1, -2$ and $\beta = 0.2, 0.4, 0.6, 0.8$ on $f(\eta)$ with $\xi_M = 5$, $\xi_{pr} = 2$, $\xi_L = 1$, $\xi_\alpha = \pm 2$

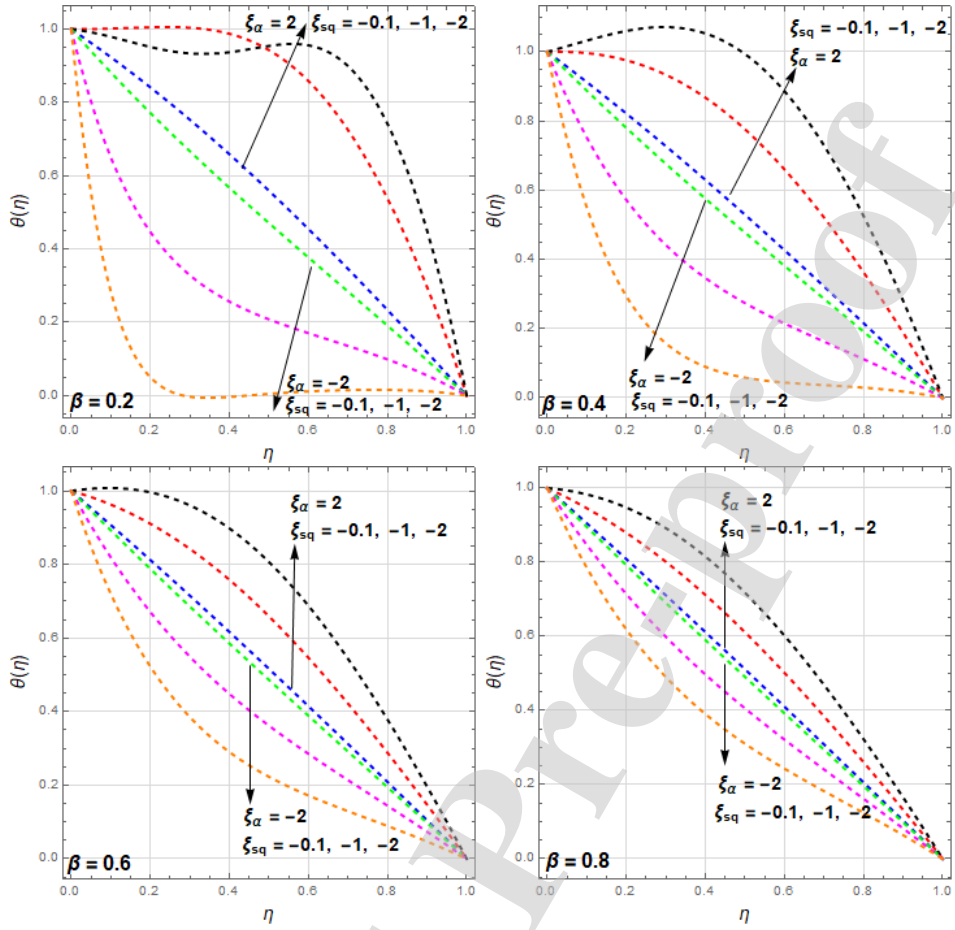

Figure 20: Impact of squeezing parameter $\xi_{sq} = -0.1, -1, -2$ and $\beta = 0.2, 0.4, 0.6, 0.8$ on $\theta(\eta)$ and $\xi_M = 5$, $\xi_{pr} = 2$, $\xi_L = 1$, $\xi_\alpha = \pm 2$

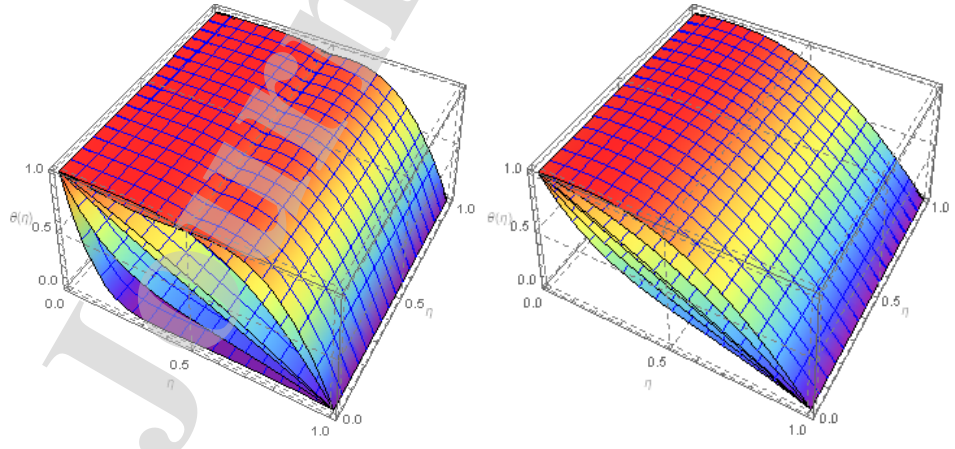

Figure 21: 3D-representation of squeezing parameter $\xi_{sq} = -0.1, -1, -2$ with $\beta = 0.2, 0.4, 0.6, 0.8$ on $\theta(\eta)$ with $\xi_M = 5$, $\xi_{pr} = 2$, $\xi_L = 1$, $\xi_\alpha = \pm 2$

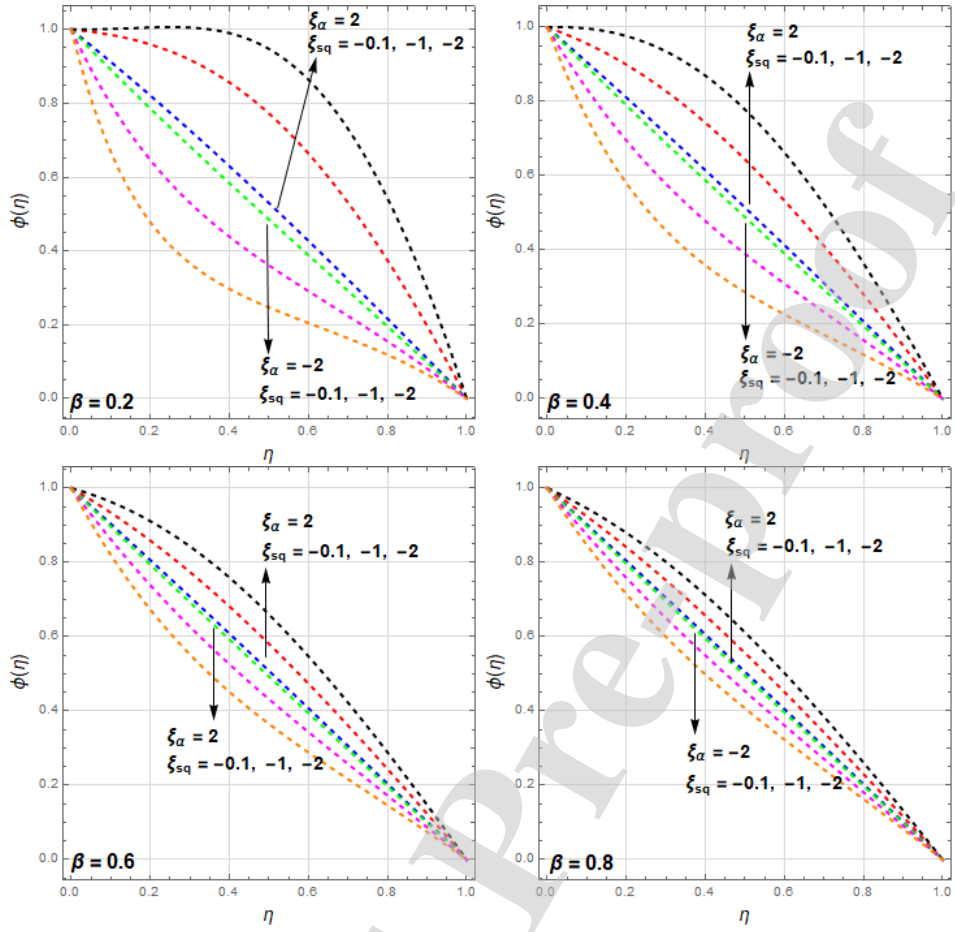

Figure 22: Impact of squeezing parameter $\xi_{sq} = -0.1, -1, -2$ and $\beta = 0.2, 0.4, 0.6, 0.8$ on $\phi(\eta)$ with $\xi_M = 5$, $\xi_{pr} = 2$, $\xi_L = 1$, $\xi_\alpha = \pm 2$

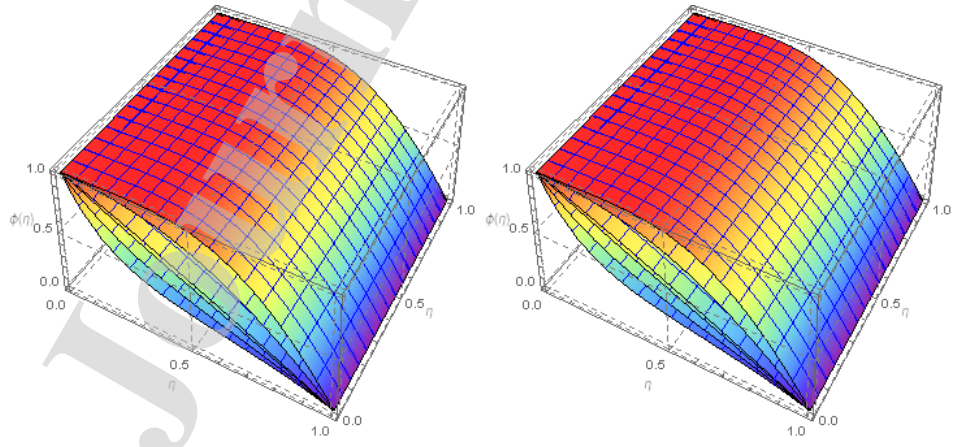

Figure 23: 3D-representation of squeezing parameter $\xi_{sq} = -0.1, -1, -2$ and $\beta = 0.2, 0.4, 0.6, 0.8$ on $\phi(\eta)$ with $\xi_M = 5$, $\xi_{pr} = 2$, $\xi_L = 1$, $\xi_\alpha = \pm 2$

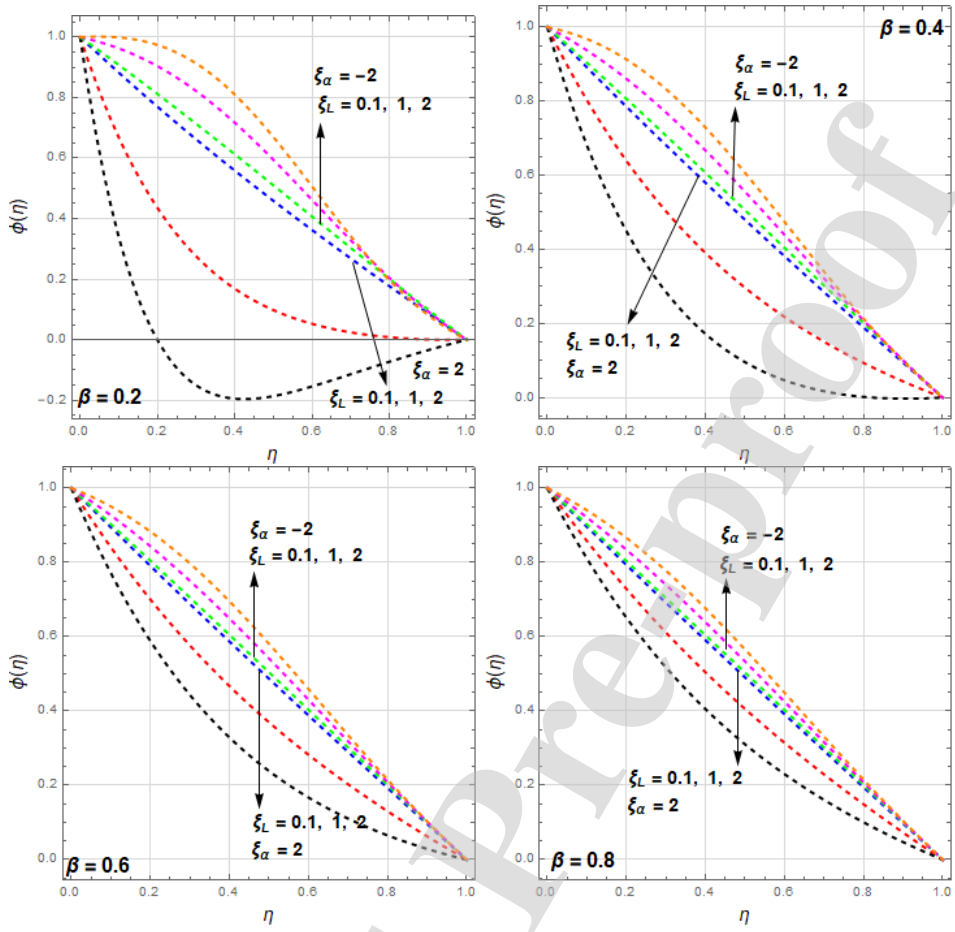

Figure 24: Impact of Lewis number $\xi_L = 0.1, 1, 2$ and $\beta = 0.2, 0.4, 0.6, 0.8$ on $\phi(\eta)$ with $\xi_{sq} = 5$, $\xi_M = 10$, $\xi_{pr} = 1$, $\xi_L = 1.5$, $\xi_\alpha = \pm 2$

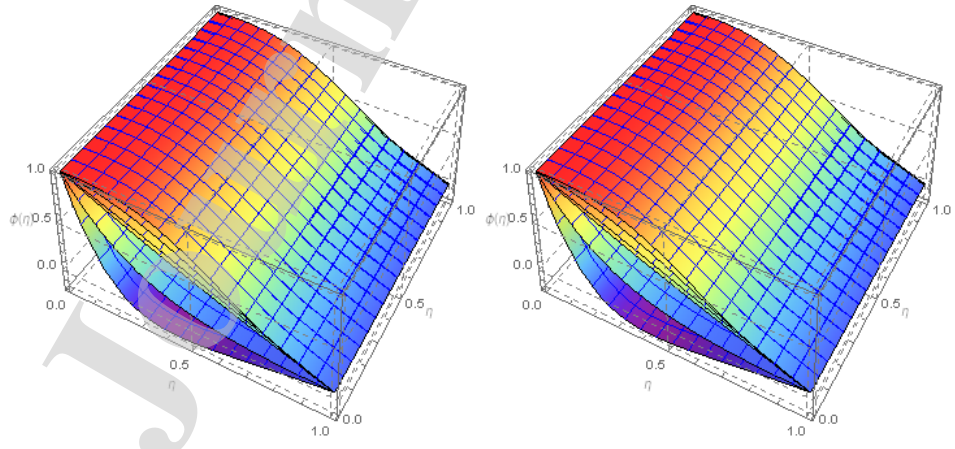

Figure 25: 3D-representation of Lewis number $\xi_L = 0.1, 1, 2$ and $\beta = 0.2, 0.4, 0.6, 0.8$ on $\phi(\eta)$ with $\xi_{sq} = 5$, $\xi_M = 10$, $\xi_{pr} = 1$, $\xi_L = 1.5$, $\xi_\alpha = \pm 2$

geometry by rotating the discs in a certain way. Because of the boundary conditions, the governing equations of this issue are changed from PDEs to ODEs. A suitable numerical methodology could be used to discover adequate boundary conditions and solve the PDEs.

- A vascular area is observed by increasing or avoiding the Hartman number. During the injection, radial Velocity may be observed to rise in the vicinity of the two disks as the viscous force decreases.
- The radial velocity is decreased when the rate of output from the flow area increases in the suction/injection parameter. Parabolic contours for both suction and injection of fluid can also be noticed by enhancing the non-Newtonian parameter.
- it is also observed that Increasing the number of Hartman reduces the vascular area and so the Lorentz force impact for small values of the non-Newtonian parameter is clearly shown.
- The influence on the flow field patterns is opposite in the suction and injection case of all physical parameters. The influence all these parameters on temperature profiles remains same.
- In suction, the temperature is directly proportional to Non-Newtonian parameters and Prandtl number and vice versa for injection.
- The small impact of Lewis numbers on the concentration profile is observed for minimum value of Non-Newtonian parameter, but it is negligible for the greater value of this parameter.
- The skin friction and heat/mass flow rate raise as the non-Newtonian parameter is increased.
- It is noticed that the influnce of Hartman number during liquid suction is minimal and also shows that the Lorentz-force has a more smooth influence on the non-Newtonian parameter.
- It is determined that in the suction scenario, raise in the non-Newtonian parameter and squeeze Reynolds number have no influence on velocity profile throughout the flow field.
- The concentration rate near the bottom disc rises steadily as the thermal diffusiveness increases.
- A rise in non-Newtonian parameter value has a minor influence on the flow field's radial and axial component.

Nomenclature

p	pressure$(N.m^{-2})$	C	dimensional concentration
r, θ, z	cylindrical polar coordinates	$\vec{r}$	radius vector of the disc
V_r	radial velocity$(m.s^{-1})$	$\vec{V}$	velocity vector
V_θ	azimuthal velocity$(m.s^{-1})$	*Greeksymbols*	
V_z	axial velocity$(m.s^{-1})$	ω	rotation vector
t	time(s)	Ω_l	lower disc angular velocity
T_u	temperature at upper disc(K)	κ	thermal conductivity(W/mK)
T_l	temperature at lower disc(K)	μ	dynamic viscosity (PaS)
C_u	concentration at upper disc	ν	kinematic viscosity(kg/mS)
C_l	concentration at lower disc	σ	relative angular velocity
Pr	Prandtl number(ν/k)	ρ	fluid density(kg/m^3)
M	Hartman Number	α	positive constant
S_q	squeezing parameter	η	similarity variable
L	Lewis Number	Γ	transformed fluid temperature
$h(t)$	distance between the two discs(m)	σ^s	stefan-Boltzmann constant
B	induced magnetic field	N_o	constant number
δ_o	Soret number	Ψ	transformed fluid concentration
ξ_α	suction/blowing parameter	κ^a	mean absorption co-efficient
c_p	specific heat of fluid(J/kgK)	*Subscript*	
D	molecular diffusion coefficient	u	fluid condition on upper disc
k_T	thermal diffusion ratio	l	fluid condition on lower disc
T_m	mean fluid temperature(K)	*Superscript*	
q_r	radiative heat flux(W/m^2)	$*$	dimensionless variable
τ_{ij}	stress components	$\prime$	derivative w.r.t η
A_1, A_2	Rivlin-Ericksen tensors		

Acknowledgements The authors extend their appreciation to the Deanship of Scientific Research at King Khalid University for funding this work through Research Group Program under Grant No. RGP. 2/51/42.

References

[1] Chhabra, R. P. (2010). Non-Newtonian fluids: an introduction. In Rheology of complex fluids (pp. 3-34). Springer, New York, NY.

[2] Abro, K. A., Atangana, A. (2020). Role of non-integer and integer order differentiations on the relaxation phenomena of viscoelastic fluid. Physica Scripta, 95(3), 035228.

[3] Farooq, A., Kamran, M., Bashir, Y., Ahmad, H., Shahzad, A., Chu, Y. M. (2020). On the flow of MHD generalized maxwell fluid via porous rectangular duct. Open Physics, 18(1), 989-1002.

[4] Abro, K. A., Siyal, A., Atangana, A. (2021). Thermal stratification of rotational second-grade fluid through fractional differential operators. Journal of Thermal Analysis and Calorimetry, 143(5), 3667-3676.

[5] Atangana, A., Jain, S. (2020). Models of fluid flowing in non-conventional media: new numerical analysis. Discrete & Continuous Dynamical Systems-S, 13(3), 467.

[6] Abro, K. A., Atangana, A. (2020). Dual fractional modeling of rate type fluid through non-local differentiation. Numerical Methods for Partial Differential Equations.

[7] Abouelregal, A. E., Ahmad, H., Yao, S. W. (2020). Functionally graded piezoelectric medium exposed to a movable heat flow based on a heat equation with a memory-dependent derivative. Materials, 13(18), 3953.

[8] Hartnett, J. P., Kostic, M. (1989). Heat transfer to Newtonian and non-Newtonian fluids in rectangular ducts. In Advances in heat transfer (Vol. 19, pp. 247-356). Elsevier.

[9] Riaz, M. B., Asif, N. A., Atangana, A., Asjad, M. I. (2019). Couette flows of a viscous fluid with slip effects and non-integer order derivative without singular kernel. Discrete and Continuous Dynamical Systems-S, 12(3), 645.

[10] Abouelregal, A. E., Ahmad, H. (2021). Thermodynamic modeling of viscoelastic thin rotating microbeam based on non-Fourier heat conduction. Applied Mathematical Modelling, 91, 973-988.

[11] Beard D., Walters K. (1964). Elastico-viscous boundary layer flows, a two-dimensional flow near a stagnation point, Proc. Cambridge Philos. Soc, vol. 60, 667-674.

[12] Serth R. (1974). Solution of a viscoelastic boundary layer equation by orthogonal collocation, J. Engrg. Math, vol. 8, pp. 89-92.

[13] Siddiqui, A. M., Irum, S., Ansari, A. R. (2008). Unsteady squeezing flow of a viscous MHD fluid between parallel plates, a solution using the homotopy perturbation method. Mathematical Modelling and Analysis, 13(4), 565-576.

[14] He, J. H., El-Dib, Y. O. (2020). Homotopy perturbation method for Fangzhu oscillator. Journal of Mathematical Chemistry, 58(10), 2245-2253.

[15] He, J. H., El-Dib, Y. O. (2021). Homotopy perturbation method with three expansions. Journal of Mathematical Chemistry, 59(4), 1139-1150.

[16] Siddiqui A, Irum S, Ansari A. (2008). Unsteady squeezing flow of a viscous MHD fluid between parallel plates, a solution using the homotopy perturbation method, Math Model Anal, vol. 2, 565-576.

[17] Ali F, Norzieha M, Sharidan M, Hayat T. (2012). New exact solutions of Stokes' second problem for an MHD second grade fluid in a porous space, International Journal of Non-Linear Mechanics, vol. 47, 521-525.

[18] Khan M., Hyder A., Haitao Q. (2009). Exact solutions for some oscillating flows of a second grade fluid with a fractional derivative model, Mathematical and Computer Modelling, vol. 49, 1519-1530.

[19] Gupta A, Rajagopal K. (1981). Flow and stability of a second grade fluid between two parallel plates rotating about noncoincident axes, Int. j. Engng Sci., vol. 19, 14O1-1409.

[20] Hayat T., Ellahi R., Asghar S., Siddiqui A. (2004). Flow induced by non-coaxial rotation of a porous disk executing non-torsional oscillations and a second grade fluid rotating at infinity, Applied Mathematical Modelling, vol. 28, pp. 591-605.

[21] Domairry G., Aziz A. (2009). Approximate analysis of MHD Squeeze flow between two parallel disks with suction or injection by homotopy perturbation method, Math. Probl. Eng., doi:10.1155/2009/603916.

[22] Rivlin R., Ericksen J. (1955). Stress deformation relation for isotropic materials, J. Ration. Mech. Anal., vol. 4, 323-425.

[23] Liao S. (2010). An optimal homotopy-analysis approach for strongly nonlinear differential equations, Commun. Nonlinear Sci. Numer. Simul., vol. 15, 2003-2016.

[24] Rashidi M., Hassan H. (2014). An analytic solution of micropolar flow in a porous channel with mass injection using homotopy analysis method, Mathematical and Computer Modeling, vol. 24, 419-437.

[25] Rashidi M, Rostami B, Freidoonimehr N and Abbasbandy S. (2014). Free convective heat and mass transfer for MHD fluid flow over a permeable vertical stretching sheet in the presence of the radiation and buoyancy effects. Ain Shams Engineering Journal 5, 901-912.

[26] Khan A, Shah R and Shuaib M. (2018). Fluid dynamics of the magnetic field dependent thermosolutal convection and viscosity between coaxial contracting discs, Results in Phys., vol. 9, 923-938.

[27] Shah R, Khan A and Shuaib M. (2018). Analysis of squeezing flow of a viscous fluid between corotating discs with Soret and Dufour effects, Heat Transfer Research, 49(11):1103-1118.

[28] Shah R, Khan A and Shuaib M. (2018). On analysis of squeezing flow between rotating discs with cross diffusion effects under the influence of coriolis and centrifugal forces, International Journal of Fluid Mechanics Research, vol. 45(4), 283-299.

- To examine Non-Newtonian fluid as a turbulent squeezing flow amongst two parallel discs
- To use the Parametric Continuation Method and BVP4c for the numerical solution
- To present the influence of the flow parameters for velocity field, heat, and mass transfer

CRediT author statement

- **Conceptualization:** Aamir Khan
- **Data curation:** Rehan A. Shah
- **Formal analysis:** M. Kamran Alam
- **Validation:** Sajid Rehman and M. Shahzad
- **Writing - original draft:** Sohail Ahmed and M. Sohail Khan
- **Funding:** Abdel-Haleem Abdel-Aty and Mohammed Zakarya
- **Writing - review editing:** Hijaz Ahmad

Declaration of interests

☐ The authors declare that they have no known competing financial interests or personal relationships that could have appeared to influence the work reported in this paper.